

Interplay between noninterfering neutrino exchange mechanisms and nuclear matrix elements in $0\nu\beta\beta$ decay

Eligio Lisi^{1,*}, Antonio Marrone^{2,1,†} and Newton Nath^{1,‡}

¹*Istituto Nazionale di Fisica Nucleare, Sezione di Bari, Via Orabona 4, 70126 Bari, Italy*

²*Dipartimento Interateneo di Fisica “Michelangelo Merlin,” Via Amendola 173, 70126 Bari, Italy*

 (Received 19 June 2023; accepted 2 September 2023; published 20 September 2023)

We revisit the phenomenology of neutrinoless double beta ($0\nu\beta\beta$) decay mediated by noninterfering exchange of light and heavy Majorana neutrinos, in the context of current and prospective ton-scale experimental searches, as well as of recent calculations of nuclear matrix elements (NME) in different nuclear models. We derive joint upper bounds on the light and heavy contributions to $0\nu\beta\beta$ decay, for different sets of NME, through separate and combined data coming from the following experiments (and isotopes): KamLAND-Zen and EXO (Xe), GERDA and MAJORANA (Ge), and CUORE (Te). We further consider three proposed projects that could provide, within current bounds, possible $0\nu\beta\beta$ decay signals at $>3\sigma$ level with an exposure of 10 ton years: nEXO (Xe), LEGEND (Ge), and CUPID (Mo). Separate and combined (Xe, Ge, Mo) signals are studied for different representative cases and NME sets, and the conditions leading to (non)degenerate light and heavy neutrino mechanisms are discussed. In particular, the role of heavy-to-light NME ratios in different isotopes is highlighted through appropriate graphical representations. By using different sets of “true” and “test” NME as a proxy for nuclear uncertainties, it is shown that the relative contributions of light and heavy neutrino exchange to $0\nu\beta\beta$ signals may be significantly biased in some cases. Implications for theoretical models connecting light and heavy Majorana neutrino masses are also briefly illustrated. These results provide further motivations to improve NME calculations, so as to better exploit the physics potential of future multi-isotope $0\nu\beta\beta$ searches at the ton scale.

DOI: [10.1103/PhysRevD.108.055023](https://doi.org/10.1103/PhysRevD.108.055023)

I. INTRODUCTION

The search for neutrinoless double beta decay ($0\nu\beta\beta$) in various (Z, A) isotopes,

$$(Z, A) \rightarrow (Z + 2, A) + 2e^-, \quad (1)$$

violating the lepton number by two units, represents a major research program in particle and nuclear physics [1–3]. The observation of such rare process would prove that neutrinos are Majorana particles [4], independently of the particle physics mechanism(s) leading to the decay, as reviewed, e.g., in [1,5,6].

Assuming the simplest mechanism involving the exchange of the three known light neutrinos, the decay half-life T_i for the isotope $i = (Z, A)$ reads

$$(T_i)^{-1} = S_i = G_i M_{\nu,i}^2 m_\nu^2, \quad (2)$$

where G_i is the phase-space factor [7,8], $M_{\nu,i}$ is the nuclear matrix element (NME) [9] and m_ν is the so-called effective Majorana mass for light ν ,

$$m_\nu = \left| \sum_{k=1}^3 U_{ek}^2 m_k \right|, \quad (3)$$

where U_{ek} is the mixing matrix element relating ν_e to the light state ν_k with mass m_k . We follow a previously adopted notation [10,11] by introducing the signal strength $S_i = 1/T_i$, and absorbing in G_i terms as $1/m_e^2$ and g_A^4 , where $g_A = 1.276$ [12] is the bare value of the axial-vector coupling. We can make contact with the alternative notation of [1], where $1/T = G_{01} g_A^4 M_{0\nu}^2 m_{\beta\beta}^2 / m_e^2$, by identifying $m_\nu = m_{\beta\beta}$, as well as $G = G_{01} g_A^4 / m_e^2$ and $M_\nu = M_{0\nu}$ for each isotope i . As in [1], we take the NME values $M_{\nu,i}$ as positive real numbers, referred to the bare value of g_A .

The pursuit of understanding the origin of possible $0\nu\beta\beta$ decay processes has led to an exploration of alternative scenarios, that could either replace or coexist with the exchange of light Majorana neutrinos ν_k [1,5,6]. Of particular importance is the exchange of heavy Majorana

*eligio.lisi@ba.infn.it

†antonio.marrone@ba.infn.it

‡newton.nath@ba.infn.it

Published by the American Physical Society under the terms of the Creative Commons Attribution 4.0 International license. Further distribution of this work must maintain attribution to the author(s) and the published article's title, journal citation, and DOI. Funded by SCOAP³.

neutrinos (N_h), that are a crucial ingredient of the celebrated seesaw mechanism [13–18], a fundamental framework aimed at addressing the smallness of neutrino masses. In this framework, heavy Majorana neutrinos may have a potential impact on various leptonic processes, including $0\nu\beta\beta$ decay.

The significance of heavy Majorana neutrinos in the context of $0\nu\beta\beta$ decay has been recognized in various studies [19–23]. The presence of both heavy (N_h) and light (ν_k) Majorana neutrinos introduces an interplay of contributions that can enrich the phenomenology of $0\nu\beta\beta$ decay. In particular, within the seesaw framework, the heavy and light neutrinos sectors are connected, and $0\nu\beta\beta$ data can constrain them jointly, at least in principle. Furthermore, low-scale left-right (LR) gauge models, a class of LR-symmetric models, have emerged as interesting candidates to generate $0\nu\beta\beta$ decay [24–30]. Such LR models have gained attention not only for their potential to explain the observed neutrino masses and mixing but also for their broader implications for unifying electroweak and strong interactions [31–33]. These models introduce new particles and interactions, e.g., right-handed (RH) currents, that could manifest in $0\nu\beta\beta$ decay as well.

A notable avenue in this quest involves considering the roles played by both ν_k and N_h [20], which find significance in many scenarios beyond the Standard Model (SM) [34]. In this context, $0\nu\beta\beta$ decay amplitudes due to both light and heavy neutrino exchange may appear, and their possible interference effects need to be considered. In this work we focus on the case of noninterfering (incoherent) contributions, that arise in phenomenologically interesting scenarios [20] and particularly in LR-symmetric models, where heavy neutrinos such as N_h are connected to RH currents through massive W_R bosons ($m_{W_R} \gg m_W \simeq 80.4$ GeV) [32,33]. For a recent investigation of the dynamics of interference suppression in LR symmetric models, see [35]. Hereafter, we assume the case of noninterfering contributions of light and heavy neutrinos to $0\nu\beta\beta$ decay; comments on interfering contributions are given below.

For noninterfering (incoherent) exchange of ν_k and N_h , Eq. (2) is generalized with the same phase space [36] as:

$$(T_i)^{-1} = S_i = G_i(M_{\nu,i}^2 m_\nu^2 + M_{N,i}^2 m_N^2), \quad (4)$$

where the $M_{N,i}$ represent the NME for heavy Majorana neutrino exchange, while m_N is another effective Majorana mass parameter for heavy N_h that, in LR models and in our notation, typically takes the form (see, e.g., [5])

$$m_N = \frac{m_W^4}{m_{W_R}^4} \left| \sum_h V_{eh}^2 \frac{m_p m_e}{M_h} \right|, \quad (5)$$

M_h being the mass of the heavy N_h , and V_{eh} the associated mixing matrix element. Hereafter, we shall take Eq. (4) as

our working hypothesis for a phenomenological analysis of current and prospective $0\nu\beta\beta$ decay data.

In principle, if the NME for both light and heavy neutrino exchange were accurately known in two different isotopes i and j , two precise experimental signals S_i and S_j would be sufficient to determine the two unknown parameters m_ν and m_N via the coupled equations

$$\begin{bmatrix} S_i G_i^{-1} \\ S_j G_j^{-1} \end{bmatrix} = \begin{bmatrix} M_{\nu,i}^2 & M_{N,i}^2 \\ M_{\nu,j}^2 & M_{N,j}^2 \end{bmatrix} \begin{bmatrix} m_\nu^2 \\ m_N^2 \end{bmatrix}, \quad (6)$$

provided that their determinant is nonzero, namely, that the heavy-to-light NME ratios are isotopically different [37],

$$\frac{M_{N,i}}{M_{\nu,i}} \neq \frac{M_{N,j}}{M_{\nu,j}}. \quad (7)$$

An additional signal in a third isotope k (with another, different NME ratio) would then act as a consistency check. Conversely, competing $0\nu\beta\beta$ mechanisms with very similar NME ratios would be largely degenerate.

Note that algebraic conditions equivalent to Eq. (7) are also required to disentangle and check interfering mechanisms, where the signal strength is of the form $S_i = G_i |M_{\nu,i} m_\nu + M_{N,i} m_N|^2$, namely, a coherent sum of amplitudes. In this case, however, additional complications arise due to the emergence of unknown relative phases among the different amplitudes, that may lead to either constructive or destructive interference, see, e.g., [38]. Various phenomenological studies, from early ones with up to four different mechanisms [39,40] to more recent investigation with two (standard plus exotic) amplitudes [41], show that cancelations play an important role in enlarging the allowed space of parameters (m_ν and M_N in our case), especially if the NME ratios lead to degeneracies. In this sense, the scenario with noninterfering (incoherent) $0\nu\beta\beta$ mechanisms considered herein is relatively simple with respect to the case of coherent mechanisms.

In practice, even this simple noninterfering scenario for a multi-isotope determination of m_ν and m_N is hindered by several problems: (i) the NME are currently affected by large uncertainties, not necessarily (all) reduced by taking ratios; (ii) the ratios $M_{N,i}/M_{\nu,i}$ happen to be quite similar in various isotopes, at least in some nuclear models; (iii) available $0\nu\beta\beta$ data are compatible with null signals while, in perspective, even positive signals may be affected by large statistical uncertainties; (iv) multi-isotope signals may lead to consistency checks (if compatible) or to unphysical solutions (if incompatible), depending in part on the assumed NME and their ratios. These and other related issues have been addressed with a variety of approaches and results in a vast literature, with emphasis on different aspects. A largely incomplete list includes studies of the algebraic NME conditions leading to (non)

degenerate mechanisms [39,40,42] or to (un)physical solutions [43], of general features of light vs heavy NME calculations [44–46], of multi-isotope NME consistency checks [47,48], of available or prospective decay rates [49–51] and of additional spectral data that may help to break degeneracies [52], just to name a few topics. It may also be noticed that the apparent similarity of NME ratios $M_{N,i}/M_{\nu,i}$ in different isotopes can be regarded, on the one hand, as a disadvantage, leading to an effective degeneracy of light and heavy mechanisms; and on the other hand as an advantage, leading to an isotope-independent generalization of Eq. (4) that interpolates between the light and heavy ν mass scales [53], covering the possible regime of intermediate masses (not considered in this work) at the Fermi momentum scale of $O(200)$ MeV.

Despite the difficulties in unraveling the above issues, $0\nu\beta\beta$ decays mediated by light and heavy neutrinos continue to attract interest, both theoretically and experimentally. Several theoretical frameworks that establish a connection between the light and heavy sectors offer the possibility of testing relationships between parameters such as m_ν and m_N in $0\nu\beta\beta$ processes. Additionally, these models link processes that violate lepton number at both low-energy and high-energy scales (e.g., at colliders [54]). For comprehensive overviews, refer to the reviews in [55,56]. Early work can be found in [24], and more recent studies are presented in [30], among many others. Concerning the NME, theoretical calculations for light and heavy neutrino exchange have been performed for a variety of candidate isotopes and nuclear models, although with still large uncertainties (as reviewed later). A general consensus is emerging about a well-defined road map to improve and stabilize the NME calculations [57,58] by benchmarking the models (possibly based on *ab initio* techniques) with as many nuclear data as possible, e.g., by exploiting NME correlations with a variety of observables [59–65]. A recent implementation of this program for ^{136}Xe suggests an encouraging reduction of the associated NME uncertainties (formally below 20% at 1σ) [66], although outstanding problems remain, such as the role of g_A quenching [67,68] or the assessment of the relative sign and size of some short-range contributions to the decay rate [69–71], with a possible different impact for light and heavy neutrino exchange.

From the experimental viewpoint, half-life constraints $T_i > 10^{25}$ y have been placed by five experiments in three isotopes: KamLAND-Zen [72] and EXO [73] (^{136}Xe), GERDA [74] and MAJORANA [75] (^{76}Ge), and CUORE [76] (^{130}Te). The next important goal will be to reach sensitivities $T_i \sim 10^{28}$ y (and possibly first signals at $>3\sigma$ level) by using detector masses of about 1 ton operating on a decadal timescale; multi-isotope searches will remain crucial to cross-check the results and to test the underlying mechanism(s) [1–3]. A prospective international program [3] envisages three ton-scale projects using

different isotopes, such as nEXO [77] (^{136}Xe), LEGEND-1000 [78] (^{76}Ge) and CUPID-1T [79] (^{100}Mo). Connecting this low-energy program with high-energy searches for heavy neutral leptons will provide complementary tests of neutrino physics beyond the standard model [80].

In this evolving context, we think it appropriate to revisit in detail several aspects of the phenomenology of $0\nu\beta\beta$ decay with noninterfering light and heavy neutrino exchange mechanisms. Our work includes a comprehensive set of recent NME from various nuclear models, a state-of-the-art analysis of both current $0\nu\beta\beta$ data and prospective decay signals in ton-scale detectors, and a discussion of the effects induced by the spread of NME (and of their heavy-to-light ν ratios), with emphasis on separate and joint bounds in the parameter space (m_ν^2, m_N^2), where phenomenological results and theoretical predictions can be usefully illustrated. In particular, we discuss the NME values and their ratios as obtained in different nuclear models for the (Xe, Ge, Te, Mo) isotopes in the last decade (Sec. II). We perform an up-to-date statistical analysis of the most constraining data from current (Xe, Ge, Te) experiments for all the NME sets (Sec. III). We also analyze prospective $0\nu\beta\beta$ signals observable at $>3\sigma$ level in ton-scale (Xe, Ge, Mo) projects, for representative NME sets and values of m_ν and m_N (Sec. IV). Effects of nuclear model uncertainties are studied by swapping “true” and “test” sets of NME values. Cases leading to (non)degenerate light-heavy neutrino mechanisms and to (un)biased or (un)physical m_ν and m_N parameters are discussed. We present illustrative tests of a theoretical model connecting m_ν and m_N (Sec. V), and finally summarize our work (Sec. VI). In our analysis, the impact of different NME ratios [as in Eq. (7)] and the interplay of different bounds are highlighted through appropriate graphical representations in terms of squared effective Majorana masses. Our findings provide additional motivations to search for $0\nu\beta\beta$ decay in different isotopes, and to improve the NME calculations for different decay mechanisms.

II. SETS OF NUCLEAR MATRIX ELEMENTS

In this work we consider fifteen sets of NME calculated in the last decade, for both light and heavy neutrino exchange in (^{136}Xe , ^{76}Ge , ^{130}Te), using different theoretical approaches and their variants: the nuclear shell model (SM) [46,81], the quasi-particle random phase approximation (QRPA) [82–84], the energy-density functional theory (EDF) [85], and the interacting boson model (IBM) [7,86]. Among these NME sets, eight include also calculations for ^{136}Mo in the QRPA, EDF, and IBM models.¹ Table I reports the adopted numerical values of the NME for light and heavy neutrino exchange (M_ν and

¹The SM approach was recently applied to ^{100}Mo [87], but only for the case of light Majorana neutrino exchange.

TABLE I. List of fifteen sets of nuclear matrix elements (NME) for $0\nu\beta\beta$ decay mediated by light neutrinos (M_ν) or heavy neutrinos (M_N), together with the M_N/M_ν ratio. The NMEs are computed in four isotopes within four different models (SM, QRPA, EDF, and IBM), and refer to the bare value $g_A = 1.276$.

NME Set	^{136}Xe			^{76}Ge			^{130}Te			^{100}Mo			Reference	Model
	M_ν	M_N	M_N/M_ν	M_ν	M_N	M_N/M_ν	M_ν	M_N	M_N/M_ν	M_ν	M_N	M_N/M_ν		
1	2.28	116	50.87	2.89	130	44.98	2.76	146	52.89				[46]	
2	2.45	167	68.16	3.07	188	61.24	2.96	210	70.95				[46]	
3	1.63	98.8	60.61	3.37	126	37.38	1.79	94.5	52.79				[81]	SM
4	1.76	143	81.25	3.57	202	56.58	1.93	136	70.46				[81]	
5	2.19	114.9	52.46	2.81	132.7	47.22	2.65	144.2	54.42				[81]	
6	1.11	66.9	60.27	3.12	187.3	60.03	2.90	191.4	66.00				[82]	
7	1.18	90.5	76.69	3.40	293.7	86.38	3.22	303.5	94.25				[82]	
8	2.91	186.3	64.02	5.26	401.3	76.29	4.00	338.3	84.57	3.9	350.8	89.95	[83]	
9	2.75	160	58.18	5.44	265	48.71	4.18	240	57.42	4.79	260	54.28	[6]	QRPA
10	3.36	172	51.19	5.82	412	70.79	4.70	385	81.91	5.15	404	78.45	[6]	
11	2.18	152	69.72	5.16	287	55.62	3.89	264	67.86	5.40	342	63.33	[84]	
12	2.46	228	92.68	5.56	433	77.87	4.37	400	91.53	5.85	508	86.84	[84]	
13	4.24	166.3	39.22	6.04	209.1	34.62	4.89	193.8	39.63	6.48	232.6	35.89	[85]	EDF
14	3.25	97.91	30.13	5.14	157.4	30.63	3.96	124.9	31.54	3.84	115.8	30.16	[86]	
15	3.40	99.17	29.17	6.34	181.6	28.65	4.15	126.8	30.56	5.07	104.1	20.54	[7]	IBM

M_N , respectively, assuming $g_A = 1.276$), as well as their ratios M_N/M_ν .

Given the crucial role of isotopically different NME ratios $M_{N,i}/M_{\nu,i}$ to avoid the degeneracy of the two mechanisms [Eq. (7)], it is useful to show such ratios for pairs of different isotopes (i, j) relevant in the analysis of current constraints ($i, j = \text{Xe, Ge, Te}$) and of prospective signals ($i, j = \text{Xe, Ge, Mo}$).

Figure 1 shows the heavy-to-light NME ratios for each pair (i, j) of isotopes among (Xe, Ge, Te). The scatter plots show a significant spread (about a factor of three in each coordinate), that reflects the still large theoretical uncertainties affecting nuclear model calculations. The points also tend to cluster around the diagonal lines, where $M_{N,i}/M_{\nu,i} = M_{N,j}/M_{\nu,j}$ and the two $0\nu\beta\beta$ decay mechanisms become degenerate. A nearly degenerate situation occurs for the IBM cases in all (i, j) pairs: in such cases, even precise measurements of $0\nu\beta\beta$ decay signals (S_i, S_j) would not be able to separate the contributions of light or heavy neutrino exchange via Eq. (6). Conversely, some QRPA and SM cases happen to be significantly off-diagonal for at least one (i, j) pair. In such cases, provided that the (unquantified) model uncertainties are small enough not to cross the diagonal line, the relative weight of the two mechanisms could be determined—at least in principle—via high-statistics (S_i, S_j) data. The EDF case provides an intermediate situation, nearly degenerate for the (Xe, Te) pair, and slightly nondegenerate for the other two isotopic pairs. Since we do not know which model is close to the “true” NME values, we must currently accept the occurrence of all possibilities about the (non)degeneracy of the light and heavy neutrino mechanisms in $0\nu\beta\beta$

searches using (Xe, Ge, Te) data. However, it is interesting to note that while the (Xe, Te) and (Xe, Ge) points are scattered on both sides of the diagonal line and along it, the (Ge, Te) ones lie only on the upper side. If this fact were not accidental, but suggestive of a model-independent inequality of the kind $(M_N/M_\nu)_{\text{Te}} > (M_N/M_\nu)_{\text{Ge}}$, then the relative amount of decays mediated by light and heavy neutrinos could be determined in principle, the better the stronger the deviation from the diagonal line.

Figure 2 shows the heavy-to-light NME ratios for each pair (i, j) among the (Xe, Ge, Mo) isotopes, relevant for future ton-scale projects in nEXO, LEGEND, and CUPID. One can make considerations similar to Fig. 1 about the overall scatter of points (large, two-sided or one-sided) and about the occurrence of (non)degenerate cases. For later purposes, each point is distinguished by the same NME set number reported in Table I (first column).

A few comments are in order, about the issues of g_A quenching [68] and additional short-range contributions [69,70] in $0\nu\beta\beta$ decay. It is still matter of debate if, in $0\nu\beta\beta$ decay, the bare value $g_A = 1.276$ should be effectively quenched by an isotope-dependent factor $q < 1$ as in other observed weak-interaction processes, reducing NMEs dominated by axial-vector components by $\sim q^2$, and thus the expected decay rates by $\sim q^4$. It may be expected that quenching effects, if any, largely cancel in the NME ratios ($M_{N,i}/M_{\nu,i}$) that govern the (non)degeneracy of light and heavy neutrino mechanisms. This can be explicitly verified for some NME calculations in Table I (numbered as 8–12, 14, and 15), where the axial NME components have been separately reported. For a typical quenching factor $q = 0.79$ (leading to $qg_A \simeq 1$) [68], we find that the NME ratios

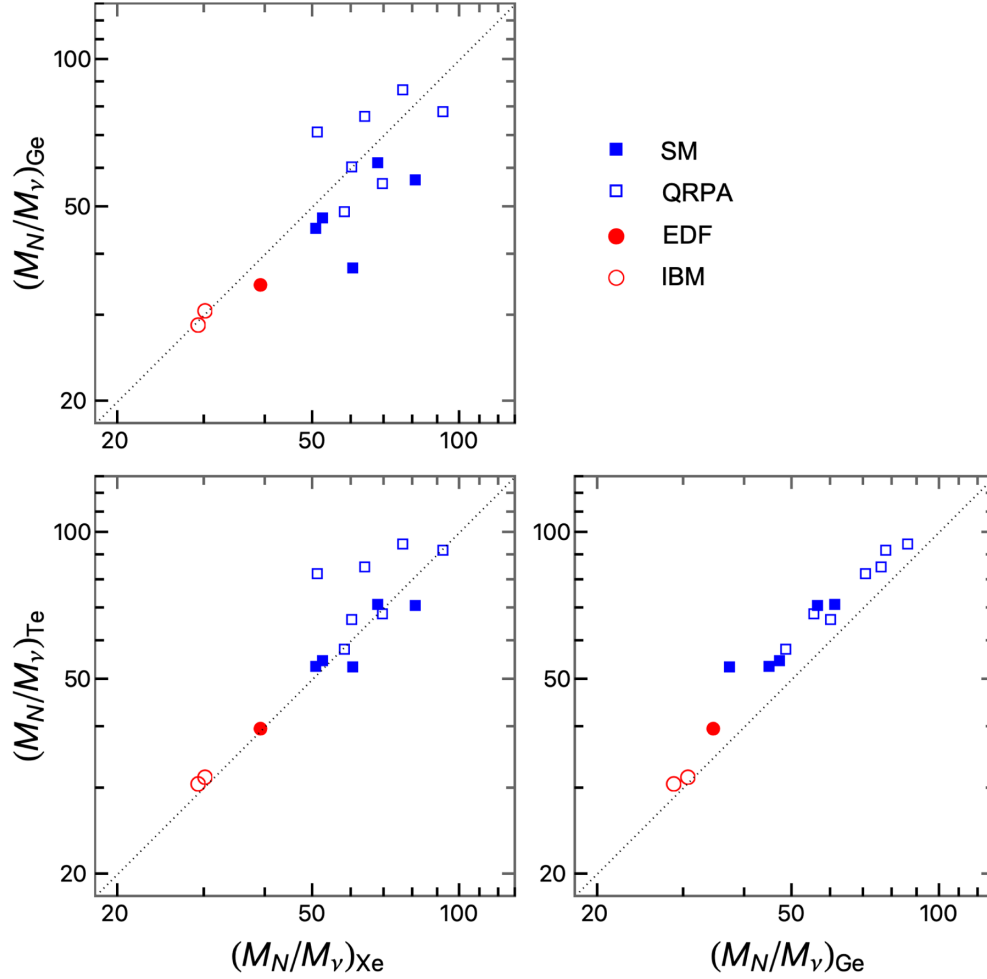


FIG. 1. Scatter plot of $M_{N,i}/M_{\nu,i}$ ratios for each pair of isotopes (i, j) among (Xe, Ge, Te). The diagonal dotted line corresponds to $M_{N,i}/M_{\nu,i} = M_{N,j}/M_{\nu,j}$. Each point refers to one of the fifteen NME sets in Table I. Different markers label different models (SM, QRPA, EDF, IBM).

are generally altered by $\lesssim 10\%$ (and only in one case by 15%), namely, by much less than the overall spread in Figs. 1 and 2. Therefore, in the presence of quenching, the qualitative results of our degeneracy analysis would not be significantly altered, although the quantitative bounds on the effective parameters m_ν and m_N would be weakened. In the absence of clear indications about quenching effects in $0\nu\beta\beta$ decay, we assume $q = 1$ for the sake of simplicity; see also related comments in [11]. Concerning recently discussed short-range effects (whose size and sign are still uncertain [71]), for different mechanisms they may contribute in different ways, not canceling in NME ratios [41]. While waiting for future progress on these issues, for the purposes of this work we surmise that the current factor-of-three spread of NMEs and of their ratios, as reported above, is already large enough to qualitatively cover the effects of “uncertain uncertainties,” such as those related to g_A quenching and short-range contributions.

We conclude this section by completing the notation related to Eq. (4). As in [11], we use the following units:

$$[m_\nu] = \text{meV}, \quad (8)$$

$$[m_N] = \text{meV}, \quad (9)$$

$$[T_i] = 10^{26} \text{ y}, \quad (10)$$

$$[S_i] = 10^{-26} \text{ y}^{-1}, \quad (11)$$

$$[G_i] = 10^{-26} \text{ y}^{-1} (\text{meV})^{-2}. \quad (12)$$

The phase space factors G_i are taken from [7] and, in our notation and units, they read:

$$G_{\text{Xe}} = 14.78 \times 10^{-6}, \quad (13)$$

$$G_{\text{Ge}} = 2.40 \times 10^{-6}, \quad (14)$$

$$G_{\text{Te}} = 14.42 \times 10^{-6}, \quad (15)$$

$$G_{\text{Mo}} = 16.15 \times 10^{-6}. \quad (16)$$

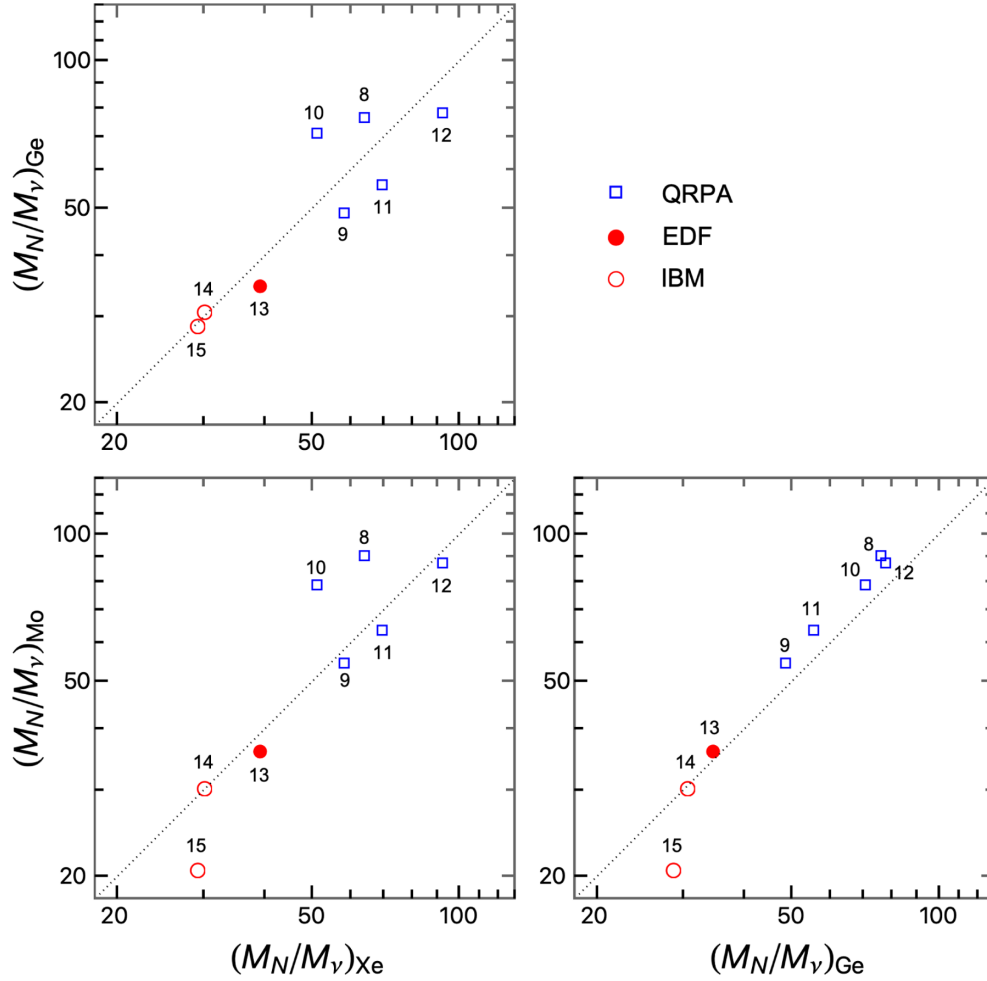


FIG. 2. As in Fig. 1, but for each pair of isotopes among (Xe, Ge, Mo), and for the NME sets numbered in Table I from 8 to 15, as reported near each point.

The G_i uncertainties are negligible in the context of this study.

III. SEPARATE AND COMBINED BOUNDS FROM CURRENT DATA

In this section we analyze the constraints on light and heavy effective neutrino masses, m_ν and m_N , as obtained by using the latest data from KamLAND-Zen [72] and EXO [73] (Xe), GERDA [74] and MAJORANA [75] (Ge), and CUORE [76] (Te).

A. Statistical data analysis

We follow the approach discussed in [10,11], by associating to each experiment a $\Delta\chi_i^2$ function of the form

$$\Delta\chi_i^2(S_i) = a_i S_i^2 + b_i S_i + c_i, \quad (17)$$

where the signal strength S is the inverse of the half-life T , see Eq. (4). Combination of data are obtained by summing

up the $\Delta\chi^2$'s. The usual 90% C.L. lower limit on T (T_{90}) is obtained by setting $\Delta\chi^2 = 2.706$.

Table II, updated from [11] with the inclusion of the final MAJORANA results [75], reports the numerical values of the (a_i, b_i, c_i) coefficients for the quoted experiments, as well as for their combination in the same isotope.² It can be noticed the combined GERDA + MAJORANA limit on the Ge half-life, $T_{90}(\text{Ge}) = 2.629 \times 10^{26}$ y, is higher than the KamLAND-Zen + EXO limit on the Xe half-life, $T_{90}(\text{Xe}) = 2.260 \times 10^{26}$ y.

Figure 3 shows the numerical information of Table II in graphical form; the left and right panels refer to separate experiments and to same-isotope combinations, respectively.

²Updated MAJORANA constraints are also quoted in [71] within the same parametrization. For KamLAND-Zen, our coefficients are based on a fit to the official $\Delta\chi^2$ profile published in the Supplemental Material of [72], and are unchanged from those reported in [11]. We note that the KamLAND-Zen coefficients in [71] are different from ours, although the same value of T_{90} is recovered.

TABLE II. Coefficients of the $\Delta\chi_i^2$ function in Eq. (17), listed according to the isotopes in the first column and the (combinations of) experiments in the second column. The next three columns report our evaluation of the coefficients (a_i, b_i, c_i) for separate experiments (upper five rows) and for their combinations in the same isotope (lower three rows). The sixth column reports our estimated 90% C.L. half-life limits T_{90} , to be compared with the official one in the seventh column (as taken from the reference in the eighth column, when applicable).

Isotope	Experiment or combination	a_i	b_i	c_i	$T_{90}/10^{26}$ y	T_{90} (expt.)	Reference
^{136}Xe	KamLAND-Zen	5.157	3.978	0.000	2.300	2.3	[72]
^{136}Xe	EXO	0.440	-0.338	0.065	0.350	0.35	[73]
^{76}Ge	GERDA	0.000	4.867	0.000	1.800	1.8	[74]
^{76}Ge	MAJORANA	0.000	2.246	0.000	0.830	0.83	[75]
^{130}Te	CUORE	0.245	-0.637	0.414	0.216	0.22	[76]
^{136}Xe	Xe (KamLAND-Zen + EXO)	5.597	3.640	0.000	2.260
^{76}Ge	Ge (GERDA + MAJORANA)	0.000	7.113	0.000	2.629
^{130}Te	Te (CUORE, as above)	0.245	-0.637	0.414	0.216	0.22	[76]

Focussing on the right panel, it should be noted that: (i) For Ge and Xe, it is $\Delta\chi^2 = 0$ at null signal, while for Te there is a weak preference for a nonzero signal; (ii) as mentioned, the Xe constraints on T are slightly weaker than those from Ge at 90% C.L.; however, they become comparatively stronger for $\Delta\chi^2 > 4.4$; (iii) in particular, at 3σ , $T_{90}(\text{Ge}) \simeq 0.8 \times 10^{26}$ y, while $T_{90}(\text{Xe}) \simeq 1 \times 10^{26}$. As emphasized in [10,11], there is a lot more information in the $\Delta\chi^2$ functions than can be captured by the parameters T_{90} , often used to characterize experimental performances.

In the following, bounds on the $0\nu\beta\beta$ effective parameters m_ν and m_N , both separately and in combination, will be obtained by summing up the $\Delta\chi_i^2$ associated to the Xe, Ge and Te signals S_i appearing in Eq. (4). For the sake of simplicity, we shall present numerical and graphical bounds only for a reference C.L. of 2σ ($\Delta\chi^2 = 4$).

B. Light neutrino exchange only: $m_\nu \geq 0$, $m_N = 0$

The case of light Majorana neutrino exchange only has a specific interest, being the simplest and most natural scenario for $0\nu\beta\beta$ decay. We update the recent analysis in [11], to account for the latest Ge data and for some differences in the adopted NME sets.³

Table III reports, in the upper half, the 2σ upper bounds on the effective light Majorana mass m_ν , for each of the fifteen representative NME sets $M_{\nu,i}$ ($i = \text{Xe, Ge, Te}$) listed in Table I. Best-fit values of m_ν are reported in the lower half. Concerning constraints from single isotopes, in most cases Xe sets the strongest 2σ bounds, followed by weaker ones from Ge and Te. However, for the cases numbered as 6 and 7 (QRPA), the NME for Xe are the lowest, and the Ge bounds prevail on those from Xe and

Te (comparable). Concerning the best fits for single isotopes, only Te data favors $m_\nu > 0$, due to the slight preference for a nonzero signal in Fig. 3, in contrast with Xe and Ge data. The combination of any two isotopes generally provides a bound stronger than the separate ones, except for the cases involving Te with relatively large NME; in such cases, the joint bounds of Te with Ge or Xe are weakened, as a result of a slight tension between the two isotopic data in terms of preferred m_ν . This effect is more evident for noted NME sets 6 and 7, where the preference for $m_\nu > 0$ at best fit persists in the Xe + Te combination. The global Xe + Ge + Te combination provides rather stable results for m_ν , characterized by $m_\nu = 0$ at best-fit values and by upper bounds $m_{\nu,2\sigma}$ stronger than any separate bound, for any choice of the NME set in Table III. The spread of NME values implies a relatively large range for the corresponding 2σ bounds,

$$m_\nu \leq m_{\nu,2\sigma} \in [43.1, 127.9] \text{ meV} \quad (\text{Xe} + \text{Ge} + \text{Te}), \quad (18)$$

that unfortunately spans a factor of three. A significant reduction of these uncertainties is expected in the future, as a results of worldwide efforts in improving the NME calculations and benchmarking the nuclear models [57,58].

C. Heavy neutrino exchange only: $m_\nu = 0$, $m_N \geq 0$

The alternative case of $0\nu\beta\beta$ decay mediated only by heavy Majorana neutrinos (or by any other nonstandard mechanism) cannot be excluded *a priori*, e.g., if a decay signal is observed, but the three complex terms in Eq. (3) interfere destructively and lead to $m_\nu \simeq 0$ (an allowed scenario for normal ordering of neutrino masses).

Table IV reports the 2σ upper limits and best fits for the effective heavy Majorana mass m_N , in the same format used in Table III for m_ν . According to Eq. (4), the m_N bounds are expected to differ from the m_ν bounds by typical NME ratios, namely, by a factor $M_N/M_\nu \simeq 30\text{--}90$ (see Fig. 1), as it indeed occurs numerically. Apart from this overall

³With respect to [11], we have added some NME calculations from studies covering both light and heavy neutrino exchange, while we have excluded those not covering the latter case. The overall number of adopted NME sets (fifteen) is accidentally the same as in [11].

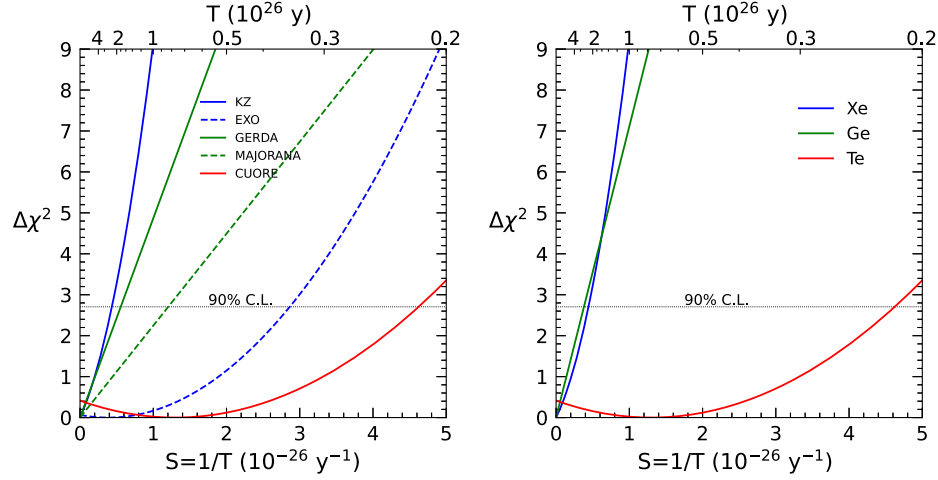


FIG. 3. $\Delta\chi^2$ functions in terms of the half-life T (top abscissa) and of the signal strength $S = 1/T$ (bottom abscissa). Left and right panels: separate experiments and their combinations for the same isotope, respectively. Dotted horizontal lines intersect the curves at 90% C.L. See the text for details.

scaling of the bounds, the previous comments about the impact of separate and combined isotopic data in Table III also apply to Table IV. The results on the 2σ upper bounds can be summarized as

$$m_N \leq m_{N,2\sigma} \in [0.75, 2.1] \text{ meV} \quad (\text{Xe} + \text{Ge} + \text{Te}). \quad (19)$$

Effective heavy Majorana masses at a scale comparable to these bounds, $m_N \sim O(1)$ meV, can be realized via Eq. (5) in LR-symmetric theories assuming favorable physics scales, such as $m_{W_R} \sim \text{few TeV}$, $M_h \in O(10^{2\pm 1})$ GeV and $V_{eh} \sim O(U_{ei})$; see [30] for a recent model construction, that will be discussed later in more detail. In general, such

models may allow comparable $0\nu\beta\beta$ contributions from both m_ν and m_N , which is the next case to be considered.

D. Noninterfering light and heavy neutrinos:

$$m_\nu \geq 0, m_N \geq 0$$

Figure 4 shows, in the upper panels, the joint upper bounds in terms of the effective Majorana mass parameters (m_ν, m_N), using separate and combined Xe, Ge and Te data from current experiments. Regions below each curve are allowed at 2σ ($\Delta\chi^2 = 4$). To avoid confusion, we show only selected cases with relatively weak or strong bounds, for seven NME sets representative of the SM, QRPA, EDF, and IBM models, numbered as in Table I. In the limits $m_N = 0$

TABLE III. Case with only light Majorana neutrino exchange ($m_\nu \geq 0, m_N = 0$). Upper half: Bounds on m_ν in meV at 2σ level from current Xe, Ge, and Te data, both separately and in combination, for each of the 15 representative NME sets listed in Table I. Lower half: Corresponding best-fit values of m_ν , in meV.

Data \ NME \rightarrow	1	2	3	4	5	6	7	8	9	10	11	12	13	14	15
Xe	86.9	80.9	121.6	112.6	90.5	178.6	168.0	68.1	72.1	59.0	90.9	80.6	46.7	61.0	58.3
Ge	167.5	157.7	143.6	135.6	172.3	155.1	142.4	92.0	89.0	83.2	93.8	87.1	80.1	94.2	76.4
Te	220.5	205.6	340.0	315.3	229.7	209.9	189.0	152.1	145.6	129.5	156.5	139.3	124.5	153.7	146.6
Xe + Ge	79.6	74.2	97.7	91.1	82.7	123.8	114.8	57.4	58.9	50.3	69.0	62.4	41.9	51.3	48.6
Xe + Te	89.6	83.4	124.9	115.7	93.3	167.5	154.5	70.4	74.5	61.0	93.4	82.8	48.1	62.9	60.1
Ge + Te	167.8	152.7	150.6	142.3	168.2	152.8	138.8	95.0	91.7	84.9	97.0	89.4	81.8	97.0	80.0
Xe + Ge + Te	82.0	76.5	100.1	93.4	85.2	127.9	118.2	59.4	61.1	52.1	71.9	65.0	43.1	55.0	50.1
Xe	0	0	0	0	0	0	0	0	0	0	0	0	0	0	0
Ge	0	0	0	0	0	0	0	0	0	0	0	0	0	0	0
Te	108.8	101.4	167.7	155.6	113.3	103.5	93.3	75.1	71.8	63.9	77.2	68.7	61.4	75.8	72.4
Xe + Ge	0	0	0	0	0	0	0	0	0	0	0	0	0	0	0
Xe + Te	0	0	0	0	0	31.7	36.0	0	0	0	0	0	0	0	0
Ge + Te	0	0	0	0	0	0	0	0	0	0	0	0	0	0	0
Xe + Ge + Te	0	0	0	0	0	0	0	0	0	0	0	0	0	0	0

TABLE IV. Case with only heavy Majorana neutrino exchange ($m_\nu = 0, m_N \geq 0$). Upper half: Bounds on m_N in meV at 2σ level from current Xe, Ge, and Te data, both separately and in combination, for each of the 15 representative NME sets listed in Tab. I. Lower half: Corresponding best-fit values of m_N , in meV.

Data \ NME \rightarrow	1	2	3	4	5	6	7	8	9	10	11	12	13	14	15
Xe	1.71	1.19	2.01	1.39	1.73	2.96	2.19	1.06	1.24	1.15	1.30	0.87	1.19	2.02	2.00
Ge	3.72	2.58	3.84	2.40	3.65	2.58	1.65	1.21	1.83	1.75	1.69	1.12	2.32	3.08	2.67
Te	4.17	2.90	6.44	4.48	4.22	3.18	2.01	1.80	2.54	1.58	2.31	1.52	3.14	4.87	4.88
Xe + Ge	1.59	1.11	1.84	1.24	1.60	2.06	1.39	0.84	1.07	0.87	1.08	0.72	1.09	1.76	1.68
Xe + Te	1.76	1.22	2.05	1.42	1.78	2.66	1.79	1.09	1.28	1.14	1.34	0.89	1.23	2.09	2.06
Ge + Te	3.36	2.33	3.98	2.51	3.35	2.44	1.55	1.22	1.81	1.15	1.66	1.10	2.28	3.15	2.78
Xe + Ge + Te	1.65	1.14	1.88	1.27	1.65	2.10	1.39	0.88	1.11	0.90	1.13	0.75	1.13	1.82	1.73
Xe	0	0	0	0	0	0	0	0	0	0	0	0	0	0	0
Ge	0	0	0	0	0	0	0	0	0	0	0	0	0	0	0
Te	2.06	1.43	3.18	2.21	2.08	1.57	0.99	0.89	1.25	0.78	1.14	0.75	1.55	2.40	2.37
Xe + Ge	0	0	0	0	0	0	0	0	0	0	0	0	0	0	0
Xe + Te	0	0	0	0	0	0.99	0.87	0	0	0	0	0	0	0	0
Ge + Te	0	0	0	0	0	0	0	0	0	0	0	0	0	0	0
Xe + Ge + Te	0	0	0	0	0	0	0	0	0	0	0	0	0	0	0

and $m_\nu = 0$, we recover the 2σ bounds reported in Tables III and IV, respectively.

The lower panels of Fig. 4 map the same bounds as in the upper panels, but in the squared variables (m_ν^2, m_N^2). Since Eq. (4) is linear in such variables, the bounds for separate Xe, Ge, Te isotopes are exactly linear in such scales. For a given NME set, the slope of the linear bound reflects the ratio $M_{N,i}/M_{\nu,i}$ for the i th isotope: the smaller the ratio, the steeper the slope. The bounds from the Xe + Ge + Te

combination stem from a best fit to a system of equations, and are not expected to be linear in principle (they should be arcs of ellipses in the squared variables). In practice, they turn out to be very close to linear, the combinations being typically dominated by a single isotope; see the rightmost lower panel in Fig. 4.

We can thus summarize the joint 2σ bounds on (m_ν^2, m_N^2) in an approximately linear parametric form, applicable to any considered NME set, and smoothly interpolating

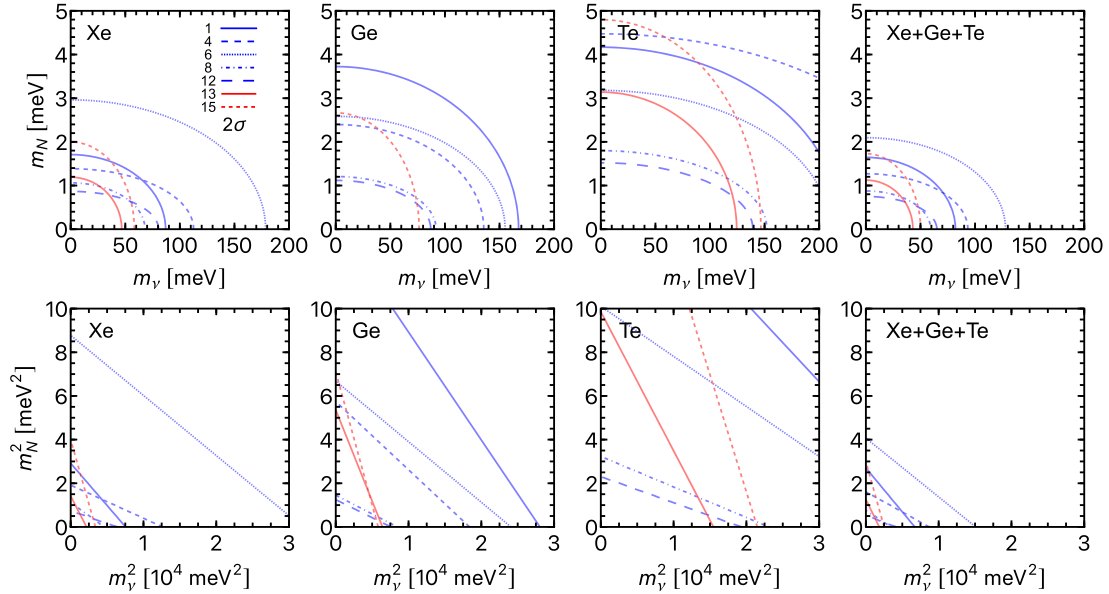


FIG. 4. Joint upper bounds on the effective Majorana masses for the exchange of light neutrinos (m_ν) and heavy neutrinos (m_N) from current Xe, Ge, and Te data, under the assumption of noninterfering exchange, Eq. (4). The legend with colored line types refers to representative NME sets, numbered as in Table I. All bounds are derived at the 2σ confidence level ($\Delta\chi^2 = 4.0$), and refer to the pairs (m_ν, m_N) and (m_ν^2, m_N^2) in the upper and lower panels, respectively. From left to right, the panels refer first to the three separate Xe, Ge and Te bounds, and then to their combination Xe + Ge + Te.

between the squares of the 2σ limits $m_{\nu,2\sigma}$ and $m_{N,2\sigma}$ reported for the Xe + Ge + Te combination in Tables III and IV, respectively:

$$m_\nu^2 \leq (1 - \alpha)m_{\nu,2\sigma}^2, \quad (20)$$

$$m_N^2 \leq \alpha m_{N,2\sigma}^2, \quad (21)$$

where $\alpha \in [0, 1]$. For $\alpha = 0$ ($\alpha = 1$), one recovers the separate bounds for the exchange of only light (heavy) Majorana neutrinos. The results discussed in this section represent the most updated bounds on noninterfering light and heavy Majorana neutrino exchange that can be derived from current multi-isotope $0\nu\beta\beta$ data and for recent NME sets.

Some comments are in order on NME uncertainties. In this work, we choose to take the spread of the results, stemming from different NME sets, as a proxy for the (largely unknown) theoretical uncertainties affecting nuclear models. In principle, more refined approaches are possible. For instance, within a nuclear model, one could construct many variants, possibly constrained by pertinent data, and infer a probability distribution function (p.d.f.) for the NME, accounting for covariances among isotopes. This approach was proposed for light Majorana neutrino exchange in [88,89], using QRPA model variants benchmarked by $2\nu\beta\beta$ data; see also the discussion in Sec. III.B of [10]. Extensions to other exchange mechanisms within the same model involve further assumptions about the joint p.d.f. of the corresponding NME, see, e.g., [90]. Furthermore, to cover also different models one must assume that the global p.d.f. of the NME can be inferred from the spread of published values, see, e.g., [41]. At present, rather than relying on a chain of assumptions about the global NME (co)variances, we prefer to stick to the scattered central values of the NME in Table I. Such a choice shall be reconsidered, if significant improvements are achieved on global NME p.d.f., covering multiple nuclear models, benchmark data, isotopes, and decay mechanisms, as envisaged in [57,58].

Finally, when passing from real data (this section) to prospective signals (next section), it should be noted that the NME sets appear in two steps, namely, in the generation of mock data (“true” NME) and in their combined fit (“test” NME). Given our ignorance of the NME set chosen by nature, we must not only allow for different true NME’s, but also for test NME’s different from the true ones. This approach was followed, e.g., in [40] to illustrate the degeneracy of multiple interfering mechanisms, and more recently in [71] to study the effect of short-range contributions to light Majorana neutrino exchange. We shall adopt a similar approach below, in selected prospective cases.

IV. ANALYSIS OF PROSPECTIVE SIGNALS IN TON-SCALE EXPERIMENTS

In the previous section, we studied upper bounds on m_ν and m_N placed by current $0\nu\beta\beta$ data for a given NME set. Should future data be consistent with no decay, the bounds would become stronger, but the qualitative aspects of our results would not change. Of course, the analysis might become more interesting in the presence of observed decays.

In this Section, we analyze selected examples of prospective $0\nu\beta\beta$ decay signals accessible at $>3\sigma$ in future ton-scale projects, with reference to nEXO (Xe), LEGEND (Ge), and CUPID (Mo), assuming a nominal exposure of 1 ton \times 10 years, together with representative NME sets from Table I. After setting the statistical tools, we discuss the reconstruction of hypothetical signals for fixed NME sets, and then study the effect of swapping true and test NME sets. The bounds will be shown in the plane charted by the squared parameters (m_ν^2, m_N^2) , in order to illustrate the constraints from single isotopes and the (non) degeneracy effects among different isotopes, related to NME ratios.

A. Statistical approach

We follow the approach advocated in [1], where a generic $0\nu\beta\beta$ search is characterized, for a given exposure \mathcal{E} , as a simple counting experiment, observing a total number of n events with respect to an average of μ events. For our purposes, the related (Poissonian) χ^2 function can be approximated as [91]:

$$\chi^2(n|\mu) \simeq 2[\mu - n + n \ln(n/\mu)]. \quad (22)$$

In general, $n = n_B + n_S$, where n_B counts the background events (assumed to be known) and n_S the signal events. The so-called discovery sensitivity, i.e., the level of rejection of the background-only hypothesis when $n_S > 0$, can be evaluated by taking $n = n_B + n_S$ and $\mu = n_B$. The so-called exclusion sensitivity, i.e., the level of rejection of a test signal n_S , if only n_B events are observed, amounts to take $n = n_B$ and $\mu = n_B + n_S$. Finally, in the general case where a (true) signal $n_{\bar{S}} > 0$ is assumed to be observed, the likelihood of an alternative (test) signal n_S corresponds to take $n = n_B + n_{\bar{S}}$ and $\mu = n_B + n_S$ in the above χ^2 .

Of course, in real $0\nu\beta\beta$ experiments, refined estimates for the likelihood of background and signal events can include further measured or simulated information (in terms of energy, time, and position), that is not contained in just two numbers (n_S and n_B). However, by appropriate choices of effective values for n_B at given exposures, one can obtain a reasonable approximation for the sensitivity to a generic signal n_S (see Table IV in [1] and Table II in [41]), as also adopted by some experimental groups for prospective studies (see, e.g., Sec. V.D.9 in [78]).

TABLE V. Poissonian χ^2 for ton-scale experiments [Eq. (25)]: reference parameters k_i and B_i and associated quantities, for a common exposure $\mathcal{E} = 10$ ton y; see the text for details. For each isotope i , the 3σ discovery half-life $T_i^{3\sigma}$ matches the one in the available design studies (as quoted in the last column).

Isotope i	Project	k_i [10^{26} y]	B_i [10^{-26} y $^{-1}$]	$T_i^{3\sigma}$ [10^{26} y]	$S_i^{3\sigma}$ [10^{-26} y $^{-1}$]	n_{B_i}	$n_{S_i}^{3\sigma}$	Reference
^{136}Xe	nEXO	622	8.84×10^{-3}	74	13.5×10^{-3}	5.50	8.41	[77]
^{76}Ge	LEGEND	403	0.99×10^{-3}	130	7.69×10^{-3}	0.40	3.10	[78]
^{100}Mo	CUPID	315	2.53×10^{-3}	80	12.5×10^{-3}	0.80	3.94	[79]

Contact with our notation is obtained, for each isotope i , by expressing n_{S_i} and n_{B_i} in terms of the signal strength S_i and associated background level B_i , respectively, via a common conversion factor k_i :

$$n_{S_i} = k_i S_i, \quad (23)$$

$$n_{B_i} = k_i B_i. \quad (24)$$

For a given exposure \mathcal{E}_i , the value of B_i (proportional to \mathcal{E}_i) determines the χ^2 function needed to test a signal S_i . In the general case mentioned above, i.e., assuming *a priori* a true signal \bar{S}_i , the χ_i^2 for any test signal S_i is given by

$$\chi_i^2(S_i) = 2k_i \left[S_i - \bar{S}_i + (B_i + \bar{S}_i) \ln \left(\frac{B_i + \bar{S}_i}{B_i + S_i} \right) \right]. \quad (25)$$

In particular, the assumption of a 3σ discovery signal $\bar{S}_i = S_i^{3\sigma}$ corresponds to have $\chi_i^2 = 9$ for $S_i = 0$ (and, of course, $\chi_i^2 = 0$ for $S_i = S_i^{3\sigma}$). A second-order expansion in $\delta = S_i - \bar{S}_i$ would provide a quadratic form, as in Eq. (17).

In this work, the B_i values have been obtained by tuning the equivalent parameters proposed in [1,41], so as to optimize the agreement with the discovery sensitivity profiles presented for various exposures in the latest 1-ton design studies by nEXO (Figs. 12 and 13 in [77]), LEGEND (Fig. 19 of [78]), and CUPID (Fig. 2 in [79]), as well as with the corresponding 3σ discovery values for the half-life ($T_i^{3\sigma} = 1/S_i^{3\sigma}$) quoted therein. Table V reports our reference values for the parameters k_i and B_i , as well as for the associated ones $T_i^{3\sigma}$, $S_i^{3\sigma}$, $n_{B_i} = k_i B_i$ and $n_{S_i}^{3\sigma} = k_i S_i^{3\sigma}$, assuming for all experiments an isotopic mass of 1 ton and 10 years of data taking, corresponding to an exposure

$$\mathcal{E}_i = \mathcal{E} = 10 \text{ ton y}. \quad (26)$$

Figure 5 shows the functions $\chi_i^2(S_i)$ for an assumed 3σ prospective signal in nEXO, LEGEND, and CUPID, as obtained from Eq. (25) by setting $\bar{S}_i = S_i^{3\sigma}$. By construction, the best fit ($\chi_i^2 = 0$), marked by a vertical dotted line, is reached for $S_i = S_i^{3\sigma}$, while the null signal $S_i = 0$ is rejected at 3σ ($\chi_i^2 = 9$). With respect to Fig. 3 (current

data), note the change of the scale in abscissa by two orders of magnitude, from typical values $T \sim O(10^{26})$ y to $\sim O(10^{28})$ y.

B. Analysis with identical (true and test) NME sets

For simplicity, we assume three representative pairs for the effective Majorana masses,

$$(\bar{m}_\nu, \bar{m}_N) = \begin{cases} (20, 0) \text{ meV} & \leftarrow \text{light } \nu_k \text{ only,} \\ (0, 0.4) \text{ meV} & \leftarrow \text{heavy } N_h \text{ only,} \\ (15, 0.3) \text{ meV} & \leftarrow \text{light } \nu_k + \text{heavy } N_h. \end{cases} \quad (27)$$

The chosen values, for any NME set considered herein, are small enough to satisfy the most stringent 2σ upper bounds placed by current data, and high enough to provide a $>3\sigma$ signal \bar{S}_i in each ton-scale experiment, where

$$\bar{S}_i = G_i (M_{\nu,i}^2 \bar{m}_\nu^2 + M_{N,i}^2 \bar{m}_N^2). \quad (28)$$

The true signals \bar{S}_i are fitted by test signals S_i via Eq. (25), both separately and in combination. We start by making the futuristic assumption that the true and test NME are the same, as if they had no uncertainty; this assumption will be dropped in the next section. As a consequence, the true values in Eq. (27) are reconstructed as best-fit test values, with $\chi^2 = \sum \chi_i^2 = 0$; what matters is the just the uncertainty of this reconstruction, that we show at the 2σ level ($\chi^2 = 4$). In the (m_ν^2, m_N^2) plane, χ^2 isolines appear as slanted bands for separate isotopes, while they appear as ellipses in multi-isotope combinations. The slopes of the bands are governed by the $M_{N,i}/M_{\nu,i}$ ratios, so that their mutual overlap (and thus the extension of the ellipse) depends of the differences among these ratios: the smaller the differences, the closer the slopes, the larger the overlap, the higher the degeneracy between the two $0\nu\beta\beta$ mechanisms.

Among the pertinent NME sets numbered from 8 to 15 in Table I and in Fig. 2, we choose four representative ones: the two QRPA sets labeled as 8 and 11, that provide relatively high ratios $M_{N,i}/M_{\nu,i}$, and appear on opposite sides of the diagonal in two of the three planes of Fig. 2; the EDF set labeled as 13, that provides intermediate values of the ratios $M_{N,i}/M_{\nu,i}$, and appears to be close to all

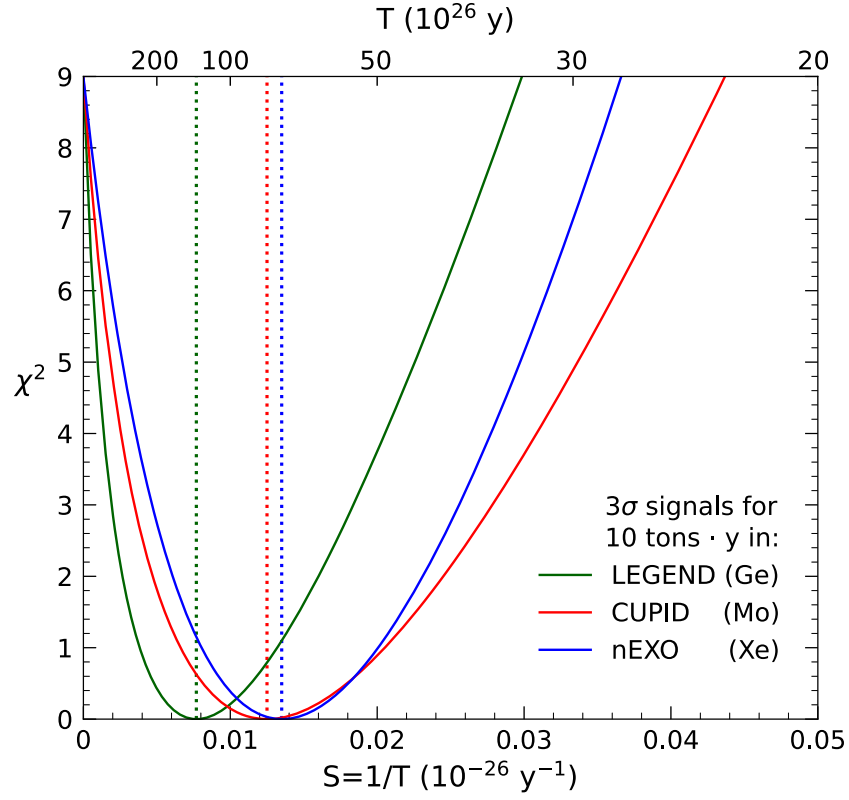


FIG. 5. Poissonian χ^2 functions in terms of the half-life T (top abscissa) and of the signal strength $S = 1/T$ (bottom abscissa), for an assumed 3σ discovery in nEXO, LEGEND and CUPID, with an exposure of 10 ton y. Each curve provides the best fit ($\chi^2 = 0$) at the corresponding discovery half-life $T^{3\sigma}$ (marked by a vertical dotted line) and rejects the test case of null signal at 3σ ($\chi^2 = 9$).

diagonals in Fig. 2; and the IBM set numbered as 15, that provides relatively low ratios $M_{N,i}/M_{\nu,i}$, significantly off-diagonal in two of the three planes of Fig. 2. The other NME sets would provide qualitatively similar results.

Figure 6 shows the 2σ constraints from ton-scale experiments for the three values of the mass parameters in Eq. (27) (left, middle, and right panels), using the QRPA NME set labeled as 8 (upper panels) and 11 (lower panels). In the upper panels, the separate bands have quite different slopes, and their combination (an ellipse) allows to distinguish at least the extreme cases. In particular, for the true cases of only light (or heavy) neutrinos, the opposite test cases of only heavy (or light) neutrinos are rejected at $>2\sigma$. For the case with both mechanisms at the same time (right panel), the limit $m_N = 0$ is rejected, while $m_\nu = 0$ is allowed, as a result of the relatively high ratio $M_{N,i}/M_{\nu,i}$ in all isotopes. In the lower panels (NME set 11), the various slopes are only moderately different, and the two mechanisms become effectively degenerate at the 2σ level: the allowed ellipse interpolates between the limiting cases and is not able to separate them.

Figure 7 is analogous to Fig. 6, but for the EDF set 13 (upper panels) and the IBM set 15 (lower panels) in Table I. These NME sets are characterized by relatively low ratios

$M_{N,i}/M_{\nu,i}$, and in comparison with those in Fig. 6 provide weaker (stronger) constraints on m_N (m_ν), reflected by the change of scale in the two coordinates. In the upper panels, the band slopes are very similar to each other, leading to an almost complete degeneracy of the two mechanisms. In the lower panels, the degeneracy is partly broken, and some limiting cases can be excluded in the 2σ combination.

The results shown in Fig. 6 and 7 show that multi-isotope searches for $0\nu\beta\beta$ decay with ton-scale experiments have the potential to statistically discriminate two noninterfering mechanisms (the exchange of light and heavy neutrinos), provided that the corresponding NME are relatively well known and have rather different ratios, in at least a couple of isotopes. For very similar NME ratios, the mechanisms are instead degenerate. The future will tell us which conditions are met by more accurate NME calculations.

C. Analysis with different (true and test) NME sets

At present, one cannot decide which NME set in Table I is the closest to the one occurring in nature for $0\nu\beta\beta$ decay (if any). This uncertainty may be accounted for by considering different NME sets for the true signals \bar{S}_i and the test signals S_i , see, e.g., [40,71]. In this approach, the best fits to the Majorana mass parameters (m_ν, m_N) will generally

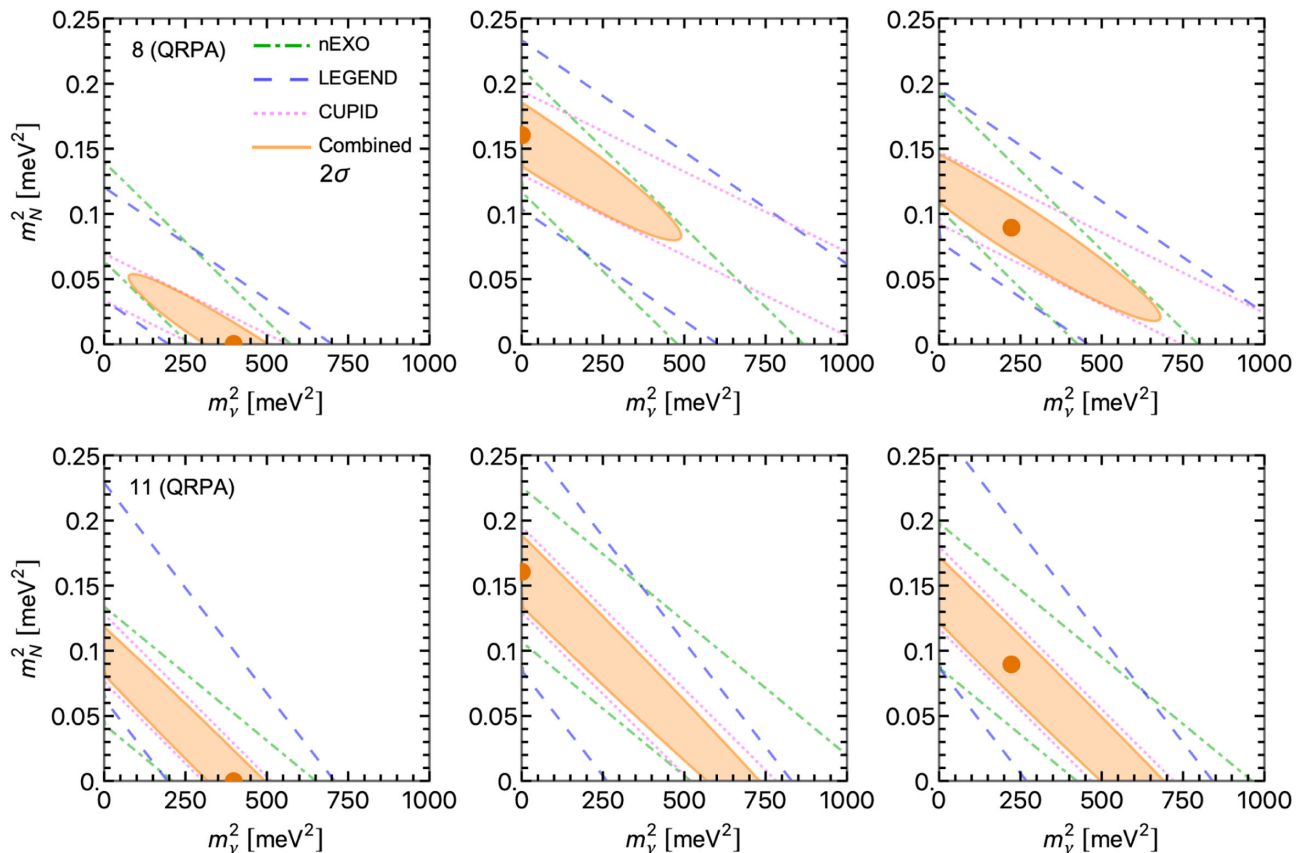


FIG. 6. Fit to prospective data from ton-scale projects (nEXO, LEGEND, CUPID), both separately (slanted bands) and in a global combination (ellipses), in the plane charted by the squared mass parameters (m_ν^2 , m_N^2), at 2σ level. The upper and lower panels refer to the NME sets numbered as 8 and 11 in Table I. The left, middle and right panels refer to the three representative cases in Eq. (27), identified by solid circles.

deviate from the true points in Eq. (27) and the minimum χ^2 will be nonzero.⁴ Values $\chi_{\min}^2 \gg 1$ would signal that the test NME provide three allowed bands allowed for (Xe, Ge, Mo) that do not intersect in the same mass parameter region, at least for physical values $m_{\nu,N}^2 \geq 0$. However, values $\chi_{\min}^2 \sim 1$ cannot exclude *a priori* unfortunate cases, where large deviations in the reconstructed parameters are present anyway.

To study the spectrum of possible outcomes, we have chosen as representative case the scenario with both light and heavy neutrino exchange, corresponding to $(m_\nu, m_N) = (15, 0.3)$ meV in Eq. (27). We have combined prospective data from ton-scale experiments, for all possible 16 pairs of true and test NME, chosen among the four sets numbered as 8, 11, 13 and 15 in Table I. The results are shown in the 16 panels of Fig. 8. Each panel is identified by a pair of (true, test) NME sets, followed by the χ_{\min}^2 value. The true values of the Majorana mass parameters are marked by a solid

circle (the same in all panels), while the reconstructed best-fit values are marked by hollow circles, surrounded by the 2σ allowed region ($\chi^2 - \chi_{\min}^2 = 4$). Solid and hollow circles coincide in the diagonal panels, where the true and test NME sets coincide, and the previous fit results (as shown in the right panels of Figs. 6 and 7) are recovered.

The twelve off-diagonal panels in Fig. 8 show a variety of possibilities. Three panels correspond to relatively low values $\chi_{\min}^2 \leq 4$, as obtained for the NME pairs (8, 15), (15, 8) and (15, 13). The corresponding outcomes are thus phenomenologically acceptable, but they show a significant bias in the reconstructed values of the Majorana mass parameters: the best fit is reached at $m_N^2 \simeq 0$ (instead of $m_N^2 = 0.09$ meV²), and the true parameters are well outside the 2σ allowed region. In particular, for the pair (15, 13) the allowed region interpolates smoothly between the limits of only light or heavy neutrino exchanges, but misses the true values for the mass parameters. For the pair (15, 8) note that, despite the significant differences between the true and test NME sets, a very good fit ($\chi_{\min}^2 \simeq 0$) is accidentally obtained. Four panels in Fig. 8 correspond to moderately high values $4 < \chi_{\min}^2 \leq 9$, as obtained for the NME pairs

⁴The value of χ_{\min}^2 should be referred to one degree of freedom, corresponding to three experimental data minus two free mass parameters.

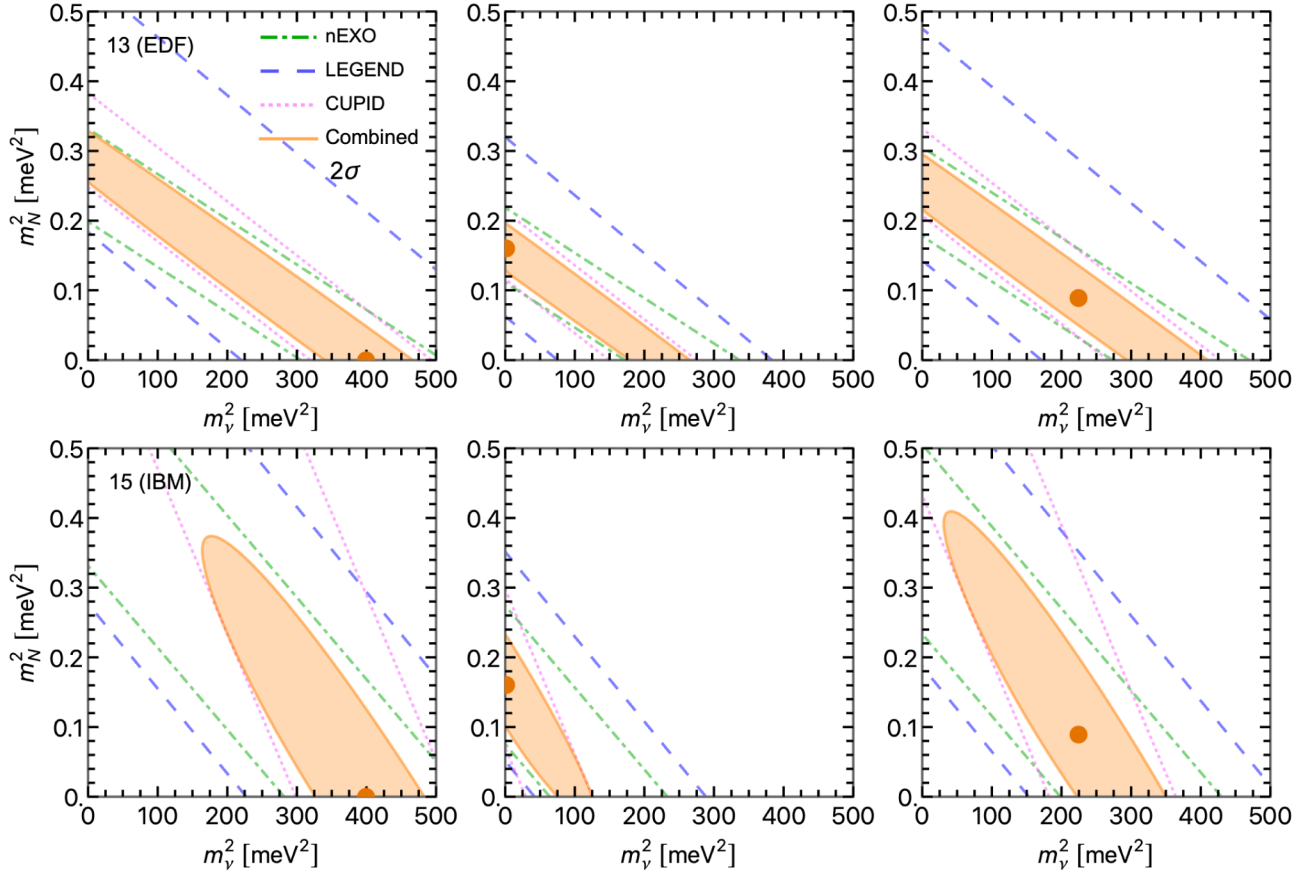


FIG. 7. As in Fig. 6, but for the NME sets numbered as as 13 and 15 in Table I.

(8, 13), (11, 8), (13, 8), and (13, 15), that provide borderline fits to the prospective data. For the first three of these pairs, the reconstructed mass parameters are within or very close to the 2σ allowed region, while for the latter pair the reconstruction bias is quite strong. Finally, five panels correspond to high values $\chi^2_{\min} > 9$, as obtained for the NME pairs (8, 11), (11, 13), (11, 15), (13, 11), and (15, 11). In such cases, it can be concluded (barring experimental systematics) that the test NME sets are unable to provide a reasonable description of the data, independently of any bias in the reconstructed parameters. In this context, having an extra constraint (three isotopic data versus two free parameters) is crucial to allow a test of the NME set [47,48]. Note also that for the pairs (11, 15) and (13, 11), having the highest χ^2_{\min} values, the allowed ellipse is not centered at the reconstructed best-fit point, and appears to be squeezed toward one axis of the panel. These features signal that the data fit would prefer unphysical values, either $m_\nu^2 < 0$ or $m_N^2 < 0$, if they were formally allowed.

In conclusion, the spread of numerical NME values in different nuclear models may be a significant source of confusion in the interpretation of future $0\nu\beta\beta$ signals from ton-scale experiments, assuming that both light and heavy neutrinos contribute to the decays. In the worst case, one

may reconstruct the underlying mass parameters with significant biases (possibly missing the true parameters), despite an apparently good fit to the data (i.e., a low χ^2_{\min}). On the opposite side, very bad fits to the data might allow to reject the chosen NME set (possibly leading to unphysical parameters). The latter test becomes possible when there are more isotopic data than free parameters. Disentangling the complex interplay between multi-isotope $0\nu\beta\beta$ searches, decay mechanisms, and assumed NME sets, will require significant progress, especially in the direction of more accurate and converging NME calculations.

Finally, we remark that if future NME calculations will reach a formal accuracy $< 20\%$, then the conditions suppressing the interference between the light and heavy neutrinos in LR models will need to be revisited, since residual interference effects [20,35], neglected herein, may become comparable to the size of NME uncertainties.

V. ILLUSTRATIVE TEST OF A THEORETICAL MODEL

In the phenomenological analysis of current and prospective $0\nu\beta\beta$ data, we have made no specific hypothesis on the effective Majorana masses m_ν and M_N , treated as free parameters. However, restrictions on the possible values of

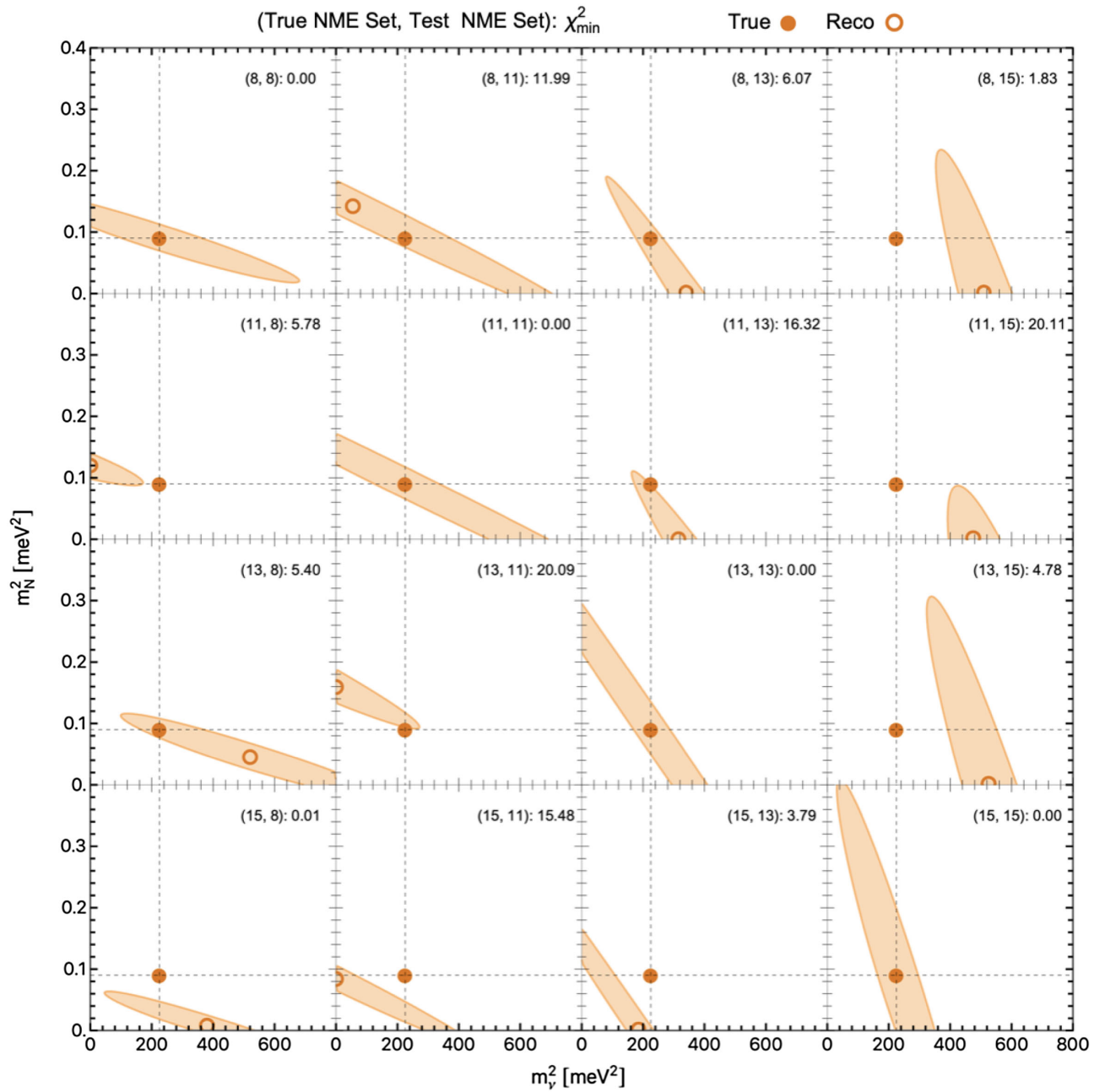


FIG. 8. Combined fit to prospective data from nEXO, LEGEND, and CUPID, assuming the case with both light and heavy neutrino exchange in Eq. (27): $(m_\nu, m_N) = (15, 0.3)$ meV. Each panel reports a pair of (true, test) NME sets, numbered as in Table I, and followed by the χ_{\min}^2 value. The true and reconstructed (m_ν^2, m_N^2) points are marked by solid and hollow circles (coinciding in the diagonal panels); the latter are surrounded by the 2σ allowed region.

m_ν come from oscillation data in normal ordering (NO) and inverted ordering (IO) for the light ν masses m_k , as a function of three unknowns, that following Eq. (3) may be chosen as the lightest neutrino mass,

$$m_L = \min \{m_k\}_{k=1,2,3}, \quad (29)$$

and two relative Majorana phases $\phi_{2,3} \in [0, 2\pi]$, with

$$\phi_k = \arg(U_{ek}^2) - \arg(U_{e1}^2), \quad (30)$$

see e.g. the review in [1]. Moreover, restrictions on admissible pairs of values (m_ν, m_N) may arise from theoretical models connecting the light and heavy neutrino sectors, such as those stemming from the seesaw mechanism [13–18]. The parameter space of these models can be probed by current joint bounds on (m_ν, m_N) , and furthermore by prospective $0\nu\beta\beta$ signals in ton-scale experiments.

Within the seesaw mechanism, the mixing between the active and sterile (heavy) neutrinos is typically expected to be $V_{eh}^2 \sim O(m_k/M_h)$ and is thus significantly suppressed, e.g., if we take $m_k \lesssim O(0.1)$ eV, based on cosmological limits on the sum of light neutrino masses [92], and $M_h \gtrsim O(1)$ GeV [56]. Larger values of V_{eh} can be attained in specific low-scale seesaw model, see e.g. [54,93–95]. A comprehensive phenomenological investigation of joint limits on M_h and V_{eh} can be found in [56] (see also [95]).

While the couplings of heavy N_h with the left-handed $(V - A)$ charged lepton current are generally small, in LR models their couplings with the right-handed $(V + A)$ current are not suppressed, and can have the same size as the active neutrino mixing matrix elements. On the other hand, the impact of the $(V + A)$ charged current interactions on observable $0\nu\beta\beta$ decay rates is subject to another kind of suppression, encapsulated by the factor $(m_W/m_{W_R})^4$ [see Eq. (5)]. For the sake of illustration, we consider a specific LR symmetric model with a double seesaw mechanism, as discussed in [30]. For alternative LR models in the context of $0\nu\beta\beta$ decay, using a type-II seesaw mechanism, see, e.g., [24,96–98].

The concerned model [30] is constructed so as to satisfy in Eq. (5) the comprehensive (M_h, V_{eh}) bounds reported in [56]. The model embeds a relatively simple structure for the heavy neutrino sector, that is governed by the parameters m_L and $\phi_{2,3}$ plus the heaviest mass

$$M_H = \max \{M_h\}_{h=1,2,3}, \quad (31)$$

where the phenomenological range $M_h \in [1, 10^3]$ GeV is assumed [30]. In particular, for each generation ($k = 1, 2, 3$) and for both NO and IO, the light and heavy neutrino masses turn out to be inversely proportional,

$$\frac{m_k}{m_L} = \frac{M_H}{M_k}, \quad (32)$$

while the mixing matrix elements are related by

$$V_{ek} = iU_{ek}^*. \quad (33)$$

Thus, the Majorana mass parameters [Eqs. (3) and (5)] admitted by the model satisfy the relation

$$m_N = \frac{m_e m_p}{m_L M_H} \left(\frac{m_W}{m_{W_R}} \right)^4 m_\nu, \quad (34)$$

corresponding to a bundle of rays in the planes charted by (m_ν, m_N) or (m_ν^2, m_N^2) .

We take the light ν oscillation parameters at their best-fit points from [10]; the effects of the associated uncertainties are minor. We also neglect the effects of further, very heavy neutrino states associated to the double seesaw structure of

the model [30]. The model space is then spanned by five free parameters, for both NO and IO:

$$m_{\nu,N} = m_{\nu,N}(m_L, M_H, m_{W_R}, \phi_2, \phi_3). \quad (35)$$

We examine a slice of this parameter space by fixing $m_{W_R} = 5.5$ TeV (the lowest limit considered in [30]) and the heaviest neutrino mass at an intermediate model value, $M_H = 300$ GeV. The remaining three parameters are randomly sampled in the intervals $\phi_{2,3} \in [0, 2\pi]$ and $m_L \in [0, 100]$ meV, where the adopted upper limit on m_L corresponds to $\sum_k m_k \simeq 300$ meV, in the ballpark of conservative upper bounds on light neutrino masses from cosmology [10]. Cases leading to heavy mass(es) $M_h < 1$ GeV are discarded. The generated model values for (m_ν^2, m_N^2) can be compared with the corresponding values allowed by either current Xe + Ge + Te data, or by future signals in Xe + Ge + Mo ton-scale experiments. For simplicity, we consider only the IBM NME set 15 in Table I, with the associated allowed regions taken from Fig. 4 (lower right panel) and Fig. 7 (lower right panel).

Figure 9 shows the results of these specific model predictions versus current data (left panel) and prospective signals (right panel), in the (m_ν^2, m_N^2) plane; note the different scales. Three representative rays [see Eq. (34)] are drawn for $m_L = 1, 3$ and 10 meV. In both panels, the sample points for NO and IO are colored in blue and cyan, respectively. The NO points are all very close to the axes, so much to be graphically unresolved in the left panel. The IO points fill a vertical stripe, that bends toward the right for vanishing m_N . In this limit, one recovers the well-known fact that m_ν is bounded from below for IO, but not for NO [1].

In the left panel of Fig. 9, points above the orange line are disfavored by current Xe + Ge + Te data at $\geq 2\sigma$ level; such points include not only NO cases with $m_N \simeq 0$ and relatively large m_ν , but also interesting IO cases with comparable $0\nu\beta\beta$ contributions from light and heavy neutrinos. Since all ray directions are allowed below the orange line, no significant $0\nu\beta\beta$ constraint can be placed on m_L .

In the right panel of Fig. 9, the axis scales (and the model point coordinates) are zoomed in by a factor of ten. The elliptic orange region is allowed at 2σ by prospective Xe + Ge + Mo data. In this example, future results tend to disfavor the IO scenario, not only in the limit of light neutrino exchange (i.e., of vanishing m_N), but also for sizeable contributions of heavy neutrinos to the $0\nu\beta\beta$ signals. They also disfavor NO cases with small m_ν , while allowing NO cases with vanishing m_N and $m_\nu^2 \simeq 220\text{--}350$ meV². The probability distribution along the ellipse major axis translates into a probability distribution for m_L , disfavoring rays with vanishing m_L .

Although the above results refer to a specific model for fixed or selected parameters, compared with representative

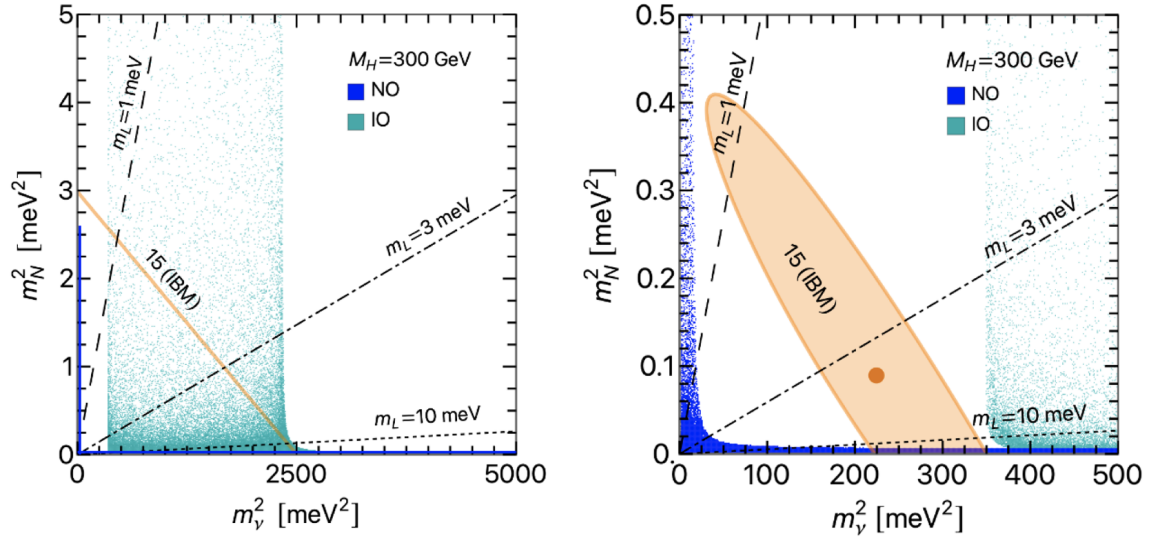


FIG. 9. Comparison of specific realizations of the model in [30] with current constraints (left panel) and future signals (right panel) at fixed NME (IBM set 15). The blue and cyan points refer to NO and IO, respectively. A few rays at constant m_L are shown. The value of M_H is set at 300 GeV. See the text for details.

phenomenological results at fixed NME, they illustrate how current and future $0\nu\beta\beta$ searches can probe heavy neutrino physics in theoretically interesting regions, that are not preempted by high-energy constraints.

VI. SUMMARY AND CONCLUSIONS

In this work, we have revisited the phenomenology of $0\nu\beta\beta$ decay mediated by noninterfering exchange of light (ν) and heavy (N) Majorana neutrinos, using current (Xe, Ge, Te) data from KamLAND-Zen, EXO, GERDA, MAJORANA, and CUORE, as well as prospective (Xe, Ge, Mo) signals in the ton-scale nEXO, LEGEND, and CUPID projects, within a state-of-the-art statistical analysis. We have highlighted the interpretation of the results in terms of recent NME sets computed in different nuclear models (SM, QRPA, EDF, and IBM). In Sec. II, we have reported available NME values for light and heavy neutrino mechanisms, and discussed the corresponding NME ratios, that are crucially connected to the (non)degeneracy of the mechanisms. In Sec. III we have derived detailed upper bounds on the effective Majorana mass parameters m_ν and m_N , using up-to-date experimental results. We have shown the usefulness of the plane (m_ν^2, m_N^2) to report joint bounds and to understand the role of NME ratios. In Sec. IV, we have considered representative cases leading to prospective $>3\sigma$ signals in ton-scale projects, for a nominal exposure of 10 ton years. Allowed regions in the (m_ν^2, m_N^2) parameters have been derived and discussed, with emphasis on (non) degenerate results. Effects of nuclear model uncertainties

have been illustrated by allowing different (true and test) sets of NME values. Cases leading to (un)biased or (un)physical m_ν and m_N parameters have been discussed. The currently large spread of NME values and ratios allows a wide spectrum of outcomes, ranging from reasonable reconstructions of the Majorana masses to more pessimistic (biased or degenerate) results, that will hopefully be restricted in the future, while the nuclear models will be improved and benchmarked. Finally, in Sec. VI, we have considered a specific theoretical model, based on left-right symmetry and connecting the light and heavy neutrino sectors. Examples of constraints on its parameter space have been shown, using both current bounds and prospective $0\nu\beta\beta$ signals. Our findings provide further motivations to pursue multi-isotope $0\nu\beta\beta$ searches at the ton mass scale, and to improve the calculations of NME needed for the interpretation of $0\nu\beta\beta$ decay data in terms of different underlying mechanisms.

ACKNOWLEDGMENTS

This work is partly supported by the Italian Ministero dell'Università e Ricerca (MUR) through the research grant No. 2017W4HA7S “NAT-NET: Neutrino and Astroparticle Theory Network” under the program PRIN 2017, and by the Istituto Nazionale di Fisica Nucleare (INFN) through the “Theoretical Astroparticle Physics” (TAsP) project. We are grateful to S. Petcov for reading the manuscript and for useful comments.

- [1] M. Agostini, G. Benato, J. A. Detwiler, J. Menéndez, and F. Vissani, Toward the discovery of matter creation with neutrinoless $\beta\beta$ decay, *Rev. Mod. Phys.* **95**, 025002 (2023).
- [2] C. Adams, K. Alfonso, C. Andreoiu, E. Angelico, I. J. Aronson, J. A. A. Asaadi, F. T. Avignone, S. N. Axani, A. S. Barabash, P. S. Barbeau *et al.*, Neutrinoless double beta decay, [arXiv:2212.11099](https://arxiv.org/abs/2212.11099).
- [3] B. Acharya, C. Adams, A. A. Aleksandrova, K. Alfonso, P. An, S. Baeßler, A. B. Balantekin, P. S. Barbeau, F. Bellini, V. Bellini *et al.*, Fundamental symmetries, neutrons, and neutrinos (FSNN): Whitepaper for the 2023 NSAC long range plan, [arXiv:2304.03451](https://arxiv.org/abs/2304.03451).
- [4] J. Schechter and J. W. F. Valle, Neutrinoless double beta decay in $SU(2) \times U(1)$ theories, *Phys. Rev. D* **25**, 2951 (1982).
- [5] W. Rodejohann, Neutrino-less double beta decay and particle physics, *Int. J. Mod. Phys. E* **20**, 1833 (2011).
- [6] J. D. Vergados, H. Ejiri, and F. Simkovic, Theory of neutrinoless double beta decay, *Rep. Prog. Phys.* **75**, 106301 (2012).
- [7] F. F. Deppisch, L. Graf, F. Iachello, and J. Kotila, Analysis of light neutrino exchange and short-range mechanisms in $0\nu\beta\beta$ decay, *Phys. Rev. D* **102**, 095016 (2020).
- [8] S. Stoica and M. Mirea, Phase space factors for double-beta decays, *Front. Phys.* **7**, 12 (2019).
- [9] J. Engel and J. Menéndez, Status and future of nuclear matrix elements for neutrinoless double-beta decay: A review, *Rep. Prog. Phys.* **80**, 046301 (2017).
- [10] F. Capozzi, E. Di Valentino, E. Lisi, A. Marrone, A. Melchiorri, and A. Palazzo, Unfinished fabric of the three neutrino paradigm, *Phys. Rev. D* **104**, 083031 (2021).
- [11] E. Lisi and A. Marrone, Majorana neutrino mass constraints in the landscape of nuclear matrix elements, *Phys. Rev. D* **106**, 013009 (2022).
- [12] B. Märkisch, H. Mest, H. Saul, X. Wang, H. Abele, D. Dubbers, M. Klopff, A. Petoukhov, C. Roick, T. Soldner *et al.*, Measurement of the Weak Axial-Vector Coupling Constant in the Decay of Free Neutrons Using a Pulsed Cold Neutron Beam, *Phys. Rev. Lett.* **122**, 242501 (2019).
- [13] P. Minkowski, $\mu \rightarrow e\gamma$ at a rate of one out of 10^9 muon decays?, *Phys. Lett.* **67B**, 421 (1977).
- [14] M. Gell-Mann, P. Ramond, and R. Slansky, Complex spinors and unified theories, *Conf. Proc. C* **790927**, 315 (1979).
- [15] T. Yanagida, Horizontal gauge symmetry and masses of neutrinos, *Conf. Proc. C* **7902131**, 95 (1979).
- [16] S. L. Glashow, The future of elementary particle physics, *NATO Sci. Ser. B* **61**, 687 (1980).
- [17] R. N. Mohapatra and G. Senjanovic, Neutrino Mass and Spontaneous Parity Nonconservation, *Phys. Rev. Lett.* **44**, 912 (1980).
- [18] J. Schechter and J. W. F. Valle, Neutrino masses in $SU(2) \times U(1)$ theories, *Phys. Rev. D* **22**, 2227 (1980).
- [19] A. Halprin, P. Minkowski, H. Primakoff, and S. P. Rosen, Double-beta decay and a massive Majorana neutrino, *Phys. Rev. D* **13**, 2567 (1976).
- [20] A. Halprin, S. T. Petcov, and S. P. Rosen, Effects of light and heavy Majorana neutrinos in neutrinoless double beta decay, *Phys. Lett.* **125B**, 335 (1983).
- [21] P. Bamert, C. P. Burgess, and R. N. Mohapatra, Heavy sterile neutrinos and neutrinoless double beta decay, *Nucl. Phys.* **B438**, 3 (1995).
- [22] A. Atre, T. Han, S. Pascoli, and B. Zhang, The search for heavy majorana neutrinos, *J. High Energy Phys.* **05** (2009) 030.
- [23] S. M. Bilenky, A. Faessler, W. Potzel, and F. Simkovic, Neutrinoless double-beta decay and seesaw mechanism, *Eur. Phys. J. C* **71**, 1754 (2011).
- [24] V. Tello, M. Nemevsek, F. Nesti, G. Senjanovic, and F. Vissani, Left-Right Symmetry: From LHC to Neutrinoless Double Beta Decay, *Phys. Rev. Lett.* **106**, 151801 (2011).
- [25] J. Barry, L. Dorame, and W. Rodejohann, Linear collider test of a neutrinoless double beta decay mechanism in left-right symmetric theories, *Eur. Phys. J. C* **72**, 2023 (2012).
- [26] J. Chakraborty, H. Z. Devi, S. Goswami, and S. Patra, Neutrinoless double- β decay in TeV scale left-right symmetric models, *J. High Energy Phys.* **08** (2012) 008.
- [27] S. P. Das, F. F. Deppisch, O. Kittel, and J. W. F. Valle, Heavy neutrinos and lepton flavour violation in left-right symmetric models at the LHC, *Phys. Rev. D* **86**, 055006 (2012).
- [28] F. F. Deppisch, C. Hati, S. Patra, P. Pritimita, and U. Sarkar, Neutrinoless double beta decay in left-right symmetric models with a universal seesaw mechanism, *Phys. Rev. D* **97**, 035005 (2018).
- [29] T. Fukuyama and T. Sato, Neutrinoless double beta decay and $\langle\eta\rangle$ mechanism in the left-right symmetric model, *J. High Energy Phys.* **06** (2023) 049.
- [30] S. Patra, S. T. Petcov, P. Pritimita, and P. Sahu, Neutrinoless double beta decay in a left-right symmetric model with a double seesaw mechanism, *Phys. Rev. D* **107**, 075037 (2023).
- [31] J. C. Pati and A. Salam, Lepton number as the fourth color, *Phys. Rev. D* **10**, 275 (1974); **11**, 703(E) (1975).
- [32] R. N. Mohapatra and J. C. Pati, A natural left-right symmetry, *Phys. Rev. D* **11**, 2558 (1975).
- [33] G. Senjanovic and R. N. Mohapatra, Exact left-right symmetry and spontaneous violation of parity, *Phys. Rev. D* **12**, 1502 (1975).
- [34] R. N. Mohapatra, S. Antusch, K. S. Babu, G. Barenboim, M. C. Chen, S. Davidson, A. de Gouvêa, P. de Holanda, B. Dutta, Y. Grossman *et al.*, Theory of neutrinos: A white paper, *Rep. Prog. Phys.* **70**, 1757 (2007).
- [35] F. Ahmed and M. Horoi, Interference effects for $0\nu\beta\beta$ decay in the left-right symmetric model, *Phys. Rev. C* **101**, 035504 (2020).
- [36] F. Simkovic, G. Pantis, J. D. Vergados, and A. Faessler, Additional nucleon current contributions to neutrinoless double beta decay, *Phys. Rev. C* **60**, 055502 (1999).
- [37] F. Deppisch and H. Pas, Pinning Down the Mechanism of Neutrinoless Double Beta Decay with Measurements in Different Nuclei, *Phys. Rev. Lett.* **98**, 232501 (2007).
- [38] S. Pascoli, M. Mitra, and S. Wong, Effect of cancellation in neutrinoless double beta decay, *Phys. Rev. D* **90**, 093005 (2014).
- [39] A. Faessler, A. Meroni, S. T. Petcov, F. Simkovic, and J. Vergados, Uncovering multiple CP -nonconserving mechanisms of $(\beta\beta)_{0\nu}$ decay, *Phys. Rev. D* **83**, 113003 (2011).
- [40] A. Faessler, G. L. Fogli, E. Lisi, A. M. Rotunno, and F. Simkovic, Multi-isotope degeneracy of neutrinoless double

- beta decay mechanisms in the quasi-particle random phase approximation, *Phys. Rev. D* **83**, 113015 (2011).
- [41] M. Agostini, F. F. Deppisch, and G. Van Goffrier, Probing the mechanism of neutrinoless double-beta decay in multiple isotopes, *J. High Energy Phys.* **02** (2023) 172.
- [42] F. Simkovic, J. Vergados, and A. Faessler, Few active mechanisms of the neutrinoless double beta-decay and effective mass of Majorana neutrinos, *Phys. Rev. D* **82**, 113015 (2010).
- [43] A. Meroni, S. T. Petcov, and F. Simkovic, Multiple CP nonconserving mechanisms of $(\beta\beta)_{0\nu}$ -decay and nuclei with largely different nuclear matrix elements, *J. High Energy Phys.* **02** (2013) 025.
- [44] L. Gráf, M. Lindner, and O. Scholer, Unraveling the $0\nu\beta\beta$ decay mechanisms, *Phys. Rev. D* **106**, 035022 (2022).
- [45] V. Cirigliano, W. Dekens, J. de Vries, M. L. Graesser, and E. Mereghetti, A neutrinoless double beta decay master formula from effective field theory, *J. High Energy Phys.* **12** (2018) 097.
- [46] J. Menéndez, Neutrinoless $\beta\beta$ decay mediated by the exchange of light and heavy neutrinos: The role of nuclear structure correlations, *J. Phys. G* **45**, 014003 (2018).
- [47] S. M. Bilenky and J. A. Grifols, The possible test of the calculations of nuclear matrix elements of the $(\beta\beta)_{0\nu}$ decay, *Phys. Lett. B* **550**, 154 (2002).
- [48] S. M. Bilenky and S. T. Petcov, Nuclear matrix elements of $0\nu\beta\beta$ decay: Possible test of the calculations, [arXiv:hep-ph/0405237](https://arxiv.org/abs/hep-ph/0405237).
- [49] V. M. Gehman and S. R. Elliott, Multiple-isotope comparison for determining $0\nu\beta\beta$ mechanisms, *J. Phys. G* **34**, 667 (2007); **35**, 029701(E) (2008).
- [50] E. Lisi, A. Rotunno, and F. Simkovic, Degeneracies of particle and nuclear physics uncertainties in neutrinoless $\beta\beta$ decay, *Phys. Rev. D* **92**, 093004 (2015).
- [51] A. Neacsu, V. A. Sevastianov, and S. Stoica, Brief review of the results regarding the possible underlying mechanisms driving the neutrinoless double beta decay, *Front. Phys.* **9**, 241 (2021).
- [52] M. Horoi and A. Neacsu, Analysis of mechanisms that could contribute to neutrinoless double-beta decay, *Phys. Rev. D* **93**, 113014 (2016).
- [53] A. Babič, S. Kovalenko, M. I. Krivoruchenko, and F. Šimkovic, Interpolating formula for the $0\nu\beta\beta$ -decay half-life in the case of light and heavy neutrino mass mechanisms, *Phys. Rev. D* **98**, 015003 (2018).
- [54] J. Kersten and A. Y. Smirnov, Right-handed neutrinos at CERN LHC and the mechanism of neutrino mass generation, *Phys. Rev. D* **76**, 073005 (2007).
- [55] F. F. Deppisch, P. S. Bhupal Dev, and A. Pilaftsis, Neutrinos and collider physics, *New J. Phys.* **17**, 075019 (2015).
- [56] P. D. Bolton, F. F. Deppisch, and P. S. Bhupal Dev, Neutrinoless double beta decay versus other probes of heavy sterile neutrinos, *J. High Energy Phys.* **03** (2020) 170.
- [57] V. Cirigliano, Z. Davoudi, W. Dekens, J. de Vries, J. Engel, X. Feng, J. Gehrlein, M. L. Graesser, L. Gráf, and H. Hergert *et al.*, Neutrinoless double-beta decay: A roadmap for matching theory to experiment, [arXiv:2203.12169](https://arxiv.org/abs/2203.12169).
- [58] V. Cirigliano, Z. Davoudi, J. Engel, R. J. Furnstahl, G. Hagen, U. Heinz, H. Hergert, M. Horoi, C. W. Johnson, A. Lovato *et al.*, Towards precise and accurate calculations of neutrinoless double-beta decay, *J. Phys. G* **49**, 120502 (2022).
- [59] E. Santopinto, H. García-Tecocoatzí, R. I. Magaña Vsevolodovna, and J. Ferretti, Heavy-ion double-charge-exchange and its relation to neutrinoless double- β decay, *Phys. Rev. C* **98**, 061601 (2018).
- [60] B. Romeo, J. Menéndez, and C. Peña Garay, $\gamma\gamma$ decay as a probe of neutrinoless $\beta\beta$ decay nuclear matrix elements, *Phys. Lett. B* **827**, 136965 (2022).
- [61] H. Ejiri, L. Jokiniemi, and J. Suhonen, Nuclear matrix elements for neutrinoless $\beta\beta$ decays and spin-dipole giant resonances, *Phys. Rev. C* **105** (2022), L022501.
- [62] J. M. Yao, I. Ginnett, A. Belley, T. Miyagi, R. Wirth, S. Bogner, J. Engel, H. Hergert, J. D. Holt, and S. R. Stroberg, Ab initio studies of the double-Gamow-Teller transition and its correlation with neutrinoless double- β decay, *Phys. Rev. C* **106**, 014315 (2022).
- [63] L. Jokiniemi, B. Romeo, P. Soriano, and J. Menéndez, Neutrinoless $\beta\beta$ -decay nuclear matrix elements from two-neutrino $\beta\beta$ -decay data, *Phys. Rev. C* **107**, 044305 (2023).
- [64] L. Jokiniemi and J. Menéndez, Correlations between neutrinoless double- β , double Gamow-Teller, and double-magnetic decays in the proton-neutron quasiparticle random-phase approximation framework, *Phys. Rev. C* **107**, 044316 (2023).
- [65] C. Jiao, C. Yuan, and J. Yao, Correlation of neutrinoless double- β decay nuclear matrix element with E2 strength, *Symmetry* **15**, 552 (2023).
- [66] M. Horoi, A. Neacsu, and S. Stoica, Predicting the neutrinoless double- β -decay matrix element of Xe136 using a statistical approach, *Phys. Rev. C* **107**, 045501 (2023).
- [67] H. Ejiri, J. Suhonen, and K. Zuber, Neutrino-nuclear responses for astro-neutrinos, single beta decays and double beta decays, *Phys. Rep.* **797**, 1 (2019).
- [68] J. T. Suhonen, Value of the axial-vector coupling strength in β and $\beta\beta$ decays: A review, *Front. Phys.* **5**, 55 (2017).
- [69] V. Cirigliano, W. Dekens, J. De Vries, M. L. Graesser, E. Mereghetti, S. Pastore, and U. Van Kolck, New Leading Contribution to Neutrinoless Double- β Decay, *Phys. Rev. Lett.* **120**, 202001 (2018).
- [70] L. Jokiniemi, P. Soriano, and J. Menéndez, Impact of the leading-order short-range nuclear matrix element on the neutrinoless double-beta decay of medium-mass and heavy nuclei, *Phys. Lett. B* **823**, 136720 (2021).
- [71] F. Pompa, T. Schwetz, and J. Y. Zhu, Impact of nuclear matrix element calculations for current and future neutrinoless double beta decay searches, *J. High Energy Phys.* **06** (2023) 104.
- [72] S. Abe *et al.* (KamLAND-Zen Collaboration), Search for the Majorana Nature of Neutrinos in the Inverted Mass Ordering Region with KamLAND-Zen, *Phys. Rev. Lett.* **130**, 051801 (2023).
- [73] G. Anton *et al.* (EXO-200 Collaboration), Search for Neutrinoless Double- β Decay with the Complete EXO-200 Dataset, *Phys. Rev. Lett.* **123**, 161802 (2019).
- [74] M. Agostini *et al.* (GERDA Collaboration), Final Results of GERDA on the Search for Neutrinoless Double- β Decay, *Phys. Rev. Lett.* **125**, 252502 (2020).
- [75] I. J. Arnquist *et al.* (Majorana Collaboration), Final Result of the Majorana Demonstrator's Search for Neutrinoless

- Double- β Decay in Ge76, *Phys. Rev. Lett.* **130**, 062501 (2023).
- [76] D. Q. Adams *et al.* (CUORE Collaboration), Search for Majorana neutrinos exploiting millikelvin cryogenics with CUORE, *Nature (London)* **604**, 53 (2022).
- [77] G. Adhikari *et al.* (nEXO Collaboration), nEXO: Neutrinoless double beta decay search beyond 10^{28} year half-life sensitivity, *J. Phys. G* **49**, 015104 (2022).
- [78] N. Abgrall *et al.* (LEGEND Collaboration), The large enriched germanium experiment for neutrinoless $\beta\beta$ decay: LEGEND-1000 preconceptual design report, [arXiv:2107.11462](https://arxiv.org/abs/2107.11462).
- [79] A. Armatol *et al.* (CUPID Collaboration), Toward CUPID-1T, [arXiv:2203.08386](https://arxiv.org/abs/2203.08386).
- [80] A. M. Abdullahi, P. B. Alzas, B. Batell, J. Beacham, A. Boyarsky, S. Carbajal, A. Chatterjee, J. I. Crespo-Anadon, F. F. Deppisch, A. De Roeck *et al.*, The present and future status of heavy neutral leptons, *J. Phys. G* **50**, 020501 (2023).
- [81] M. Horoi and A. Neacsu, Shell model predictions for ^{124}Sn double- β decay, *Phys. Rev. C* **93**, 024308 (2016).
- [82] D. L. Fang, A. Faessler, and F. Simkovic, $0\nu\beta\beta$ -decay nuclear matrix element for light and heavy neutrino mass mechanisms from deformed quasiparticle random-phase approximation calculations for ^{76}Ge , ^{82}Se , ^{130}Te , ^{136}Xe , and ^{150}Nd with isospin restoration, *Phys. Rev. C* **97**, 045503 (2018).
- [83] J. Hyvärinen and J. Suhonen, Nuclear matrix elements for $0\nu\beta\beta$ decays with light or heavy Majorana-neutrino exchange, *Phys. Rev. C* **91**, 024613 (2015).
- [84] A. Faessler, M. González, S. Kovalenko, and F. Šimkovic, Arbitrary mass Majorana neutrinos in neutrinoless double beta decay, *Phys. Rev. D* **90**, 096010 (2014).
- [85] L. S. Song, J. M. Yao, P. Ring, and J. Meng, Nuclear matrix element of neutrinoless double- β decay: Relativity and short-range correlations, *Phys. Rev. C* **95**, 024305 (2017).
- [86] J. Barea, J. Kotila, and F. Iachello, $0\nu\beta\beta$ and $2\nu\beta\beta$ nuclear matrix elements in the interacting boson model with isospin restoration, *Phys. Rev. C* **91**, 034304 (2015).
- [87] L. Coraggio, N. Itaco, G. De Gregorio, A. Gargano, R. Mancino, and F. Nowacki, Shell-model calculation of ^{100}Mo double- β decay, *Phys. Rev. C* **105**, 034312 (2022).
- [88] A. Faessler, G. L. Fogli, E. Lisi, V. Rodin, A. M. Rotunno, and F. Simkovic, QRPA uncertainties and their correlations in the analysis of $0\nu\beta\beta$ decay, *Phys. Rev. D* **79**, 053001 (2009).
- [89] A. Faessler, G. L. Fogli, E. Lisi, V. Rodin, A. M. Rotunno, and F. Simkovic, Addendum to: Quasiparticle random phase approximation uncertainties and their correlations in the analysis of $0\nu\beta\beta$ decay, *Phys. Rev. D* **87**, 053002 (2013).
- [90] S. F. Ge, W. Rodejohann, and K. Zuber, Half-life expectations for neutrinoless double beta decay in standard and non-standard scenarios, *Phys. Rev. D* **96**, 055019 (2017).
- [91] R. L. Workman *et al.* (Particle Data Group), Review of particle physics, *Prog. Theor. Exp. Phys.* **2022**, 083C01 (2022).
- [92] N. Aghanim *et al.* (Planck Collaboration), Planck 2018 results. VI. Cosmological parameters, *Astron. Astrophys.* **641**, A6 (2020); **652**, C4(E) (2021).
- [93] A. Pilaftsis, Radiatively induced neutrino masses and large Higgs neutrino couplings in the standard model with Majorana fields, *Z. Phys. C* **55**, 275 (1992).
- [94] X. G. He, S. Oh, J. Tandean, and C. C. Wen, Large mixing of light and heavy neutrinos in seesaw models and the LHC, *Phys. Rev. D* **80**, 073012 (2009).
- [95] M. Mitra, G. Senjanovic, and F. Vissani, Neutrinoless double beta decay and heavy sterile neutrinos, *Nucl. Phys.* **B856**, 26 (2012).
- [96] P. S. Bhupal Dev, S. Goswami, M. Mitra, and W. Rodejohann, Constraining neutrino mass from neutrinoless double beta decay, *Phys. Rev. D* **88**, 091301 (2013).
- [97] S. F. Ge, M. Lindner, and S. Patra, New physics effects on neutrinoless double beta decay from right-handed current, *J. High Energy Phys.* **10** (2015) 077.
- [98] G. Li, M. Ramsey-Musolf, and J. C. Vasquez, Left-Right Symmetry and Leading Contributions to Neutrinoless Double Beta Decay, *Phys. Rev. Lett.* **126**, 151801 (2021).